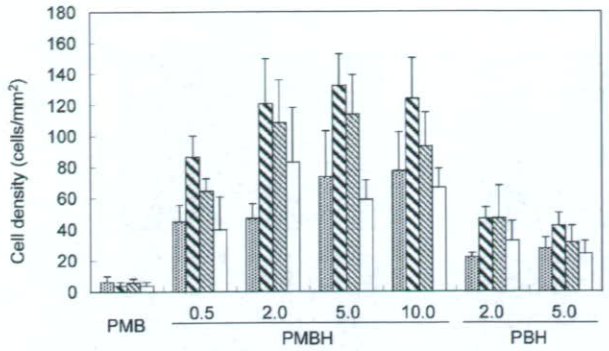

Figure 6. Surface density of ManLev-treated HL-60 cells adhered to polymer surfaces. Filled column: 15 min, deep stripe column: 2 h, light stripe column: 4 h, open column: 24 h.

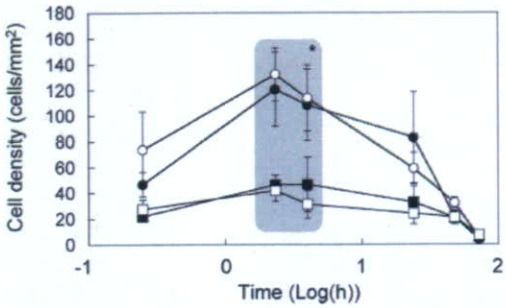

Figure 7. Time-dependence of cell density on PMHB and PBH. Filled circle: PMBH2, open circle: PMBH5, filled square: PBH2, open square: PBH5. * $p < 0.01$ PMBH vs PBH.

surface mole fraction of MH units was determined from the XPS elemental concentration, and the amount was almost constant regardless of the bulk concentration when the MH unit mole fraction in the feed was more than 2 mol %, as shown in Table 1. The water contact angles of the polymer surface are summarized in Table 2. The receding contact angle for the MPC polymers was lower than those for PBH and PBMA. MH unit mole fractions within the range of 2−5 mol % did not affect the water contact angles.

A phosphorylcholine surface with hydrazide groups was prepared by coating a PET plate with PMBH.

Attachment of HL-60 Cells to a Polymer Surface. In this study, HL-60 cells were used as typical nonadhesive cells. The expression of ketone groups on the cell surface was confirmed by treatment with Alexa Fluor 350 hydrazide. This compound stained the cell membrane of ManLev-treated HL-60 cells, but not that of ManLev-untreated HL-60 cells, as shown in Figure 4.

Figure 5 shows phase-contrast micrographs of the polymer surfaces after incubation (2 h) with HL-60 cells that had been pretreated with or without ManLev. ManLev-untreated HL-60 cells did not attach to any of the polymer surfaces. ManLev-treated HL-60 cells did not attach to the control PMB surface. In contrast, ManLev-treated HL-60 cells attached to both the PMBH and PBH surfaces.

The surface densities of adherent cells on polymer surfaces as a function of time after incubation are summarized in Figures 6 and 7. On polymer surfaces with hydrazide groups, cell attachment occurred after 15 min of incubation and the density was stable for 2 h. The density of cells attached to PMBH surfaces increased with an increase in the surface mole fraction of MH units.

The number of HL-60 cells attached to PMBH decreased after 24 h of incubation, as shown in Figure 7.

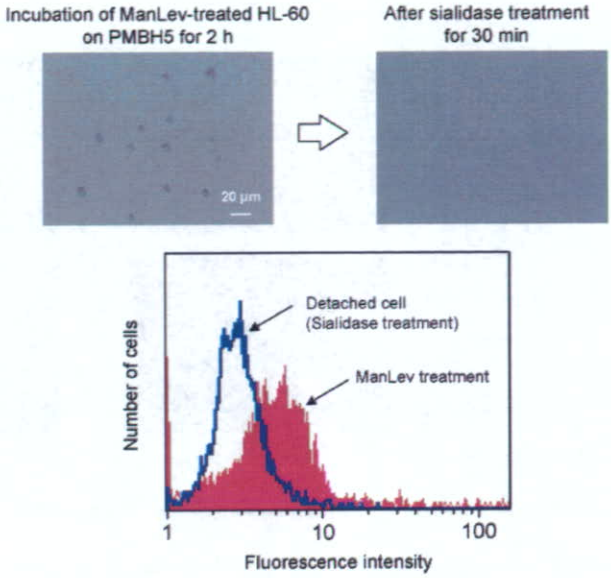

Figure 8. Effect of sialidase treatment on ManLev-treated HL-60 cells attached on PMBH5.

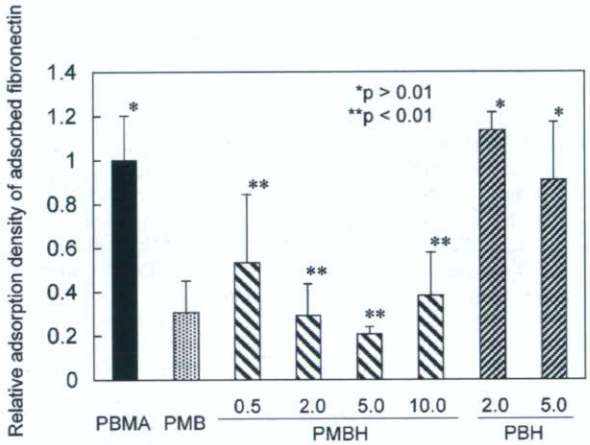

Figure 9. Relative density of fibronectin adsorbed on polymer surfaces from 10% FBS. PBMA = 1.0.

The cell-surface ketone groups decreased to 50% of their initial level at 48 h (*21*). Cell attachment was affected by the density of cell-surface ketone groups. On the other hand, the detachment of cells from the PBH surface was not observed until 48 h of incubation. The metabolic function of HL-60 cells attached to PBH may be affected by the surface. After 72 h of incubation, almost all of the attached cells were detached from the polymer surfaces.

The reactivity of ketone groups on a cell surface with hydrazide groups was confirmed in previous reports (*20*, *43*). In addition, ManLev-treated HL-60 cells did not attach to PMBH or PBH upon further incubation in fresh medium (without ManLev) for 3 days before contact with the polymers (data not shown) because of the depletion of ketone groups from the cell surfaces. The detachment of cells from PMBH by enzyme treatment for 30 min, every cell was detached from the PMBH5 surface as shown in Figure 8. The surface density of ketone groups on the cell membrane of cells detached from a polymer surface was lower than that of ManLev-treated cells. All of these results suggest that cells attached to polymer surfaces through the reaction of ketone groups in carbo-

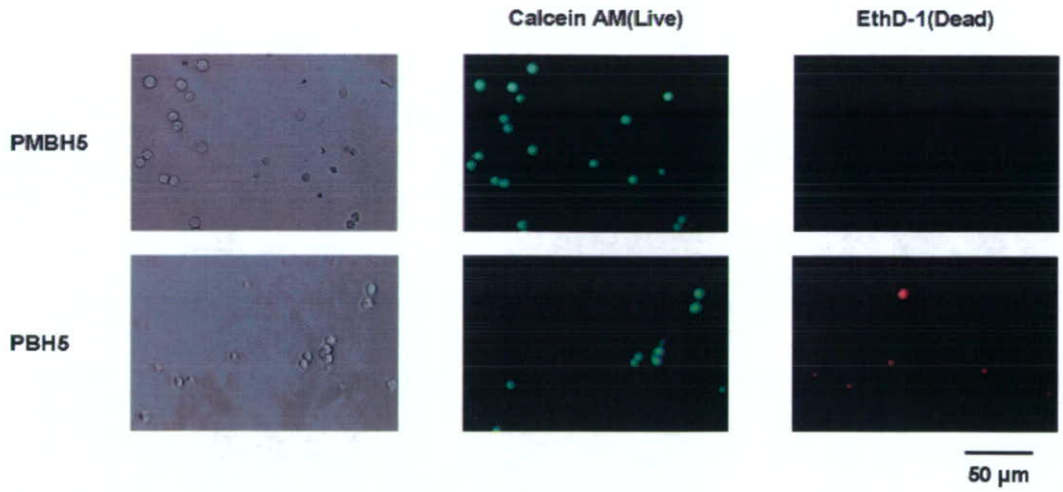

Figure 10. Micrographs of viability of adherent cells on polymer surfaces.

hydrates on the cell surface and hydrazide groups on the polymer surface.

The PMBH surface showed a much greater attachment of cells than the PBH surface, even with the same amount of hydrazide groups. The density on PMBH was approximately three times greater ($p < 0.01$ at 2 and 4 h of incubation) than that on PBH, as shown in Figure 7.

We also studied interaction between MPC polymer and plasma protein. When the mole fraction of MPC units in a polymer was around 0.3, nonspecific protein adsorption was effectively reduced and the extent of adsorption from human plasma was approximately 0.4 $\mu g/cm^2$, which is lower than the extent of monolayer adsorption of albumin (lit. 0.9 $\mu g/cm^2$) (*38*, *44*). In contrast, the amount of protein adsorbed on PBMA was more than 1.0 $\mu g/cm^2$. It has also been clarified that protein in contact with MPC polymer does not undergo denaturation (*39*). We measured the amount of serum protein adsorbed on polymer surfaces to better understand the difference in cell adhesion on PMBH and PBH. As shown in Figure 9, the amount of fibronectin adsorbed onto PBH was the same as that adsorbed onto PBMA, but was significantly greater than that on PMBH. Thus, on the PBH surface, the amount of adsorbed serum proteins would be greater than the amount of monolayer adsorption.

The hydrazide groups on the PMBH surface were not covered with serum protein, and these groups are effective for recognition of the cell surface. On the other hand, the adsorbed proteins on PBH hid hydrazide groups on the polymer, which resulted in a decrease in the density of cell attachment because the surface properties of PBH were similar to those of PBMA (Table 2), which shows a large amount of protein adsorption from plasma (*38*). The PMBH surface could effectively catch HL-60 cells and did not have an adverse effect on cell function.

Viability of Cells Attached to a Polymer Surface. Figure 10 shows phase-contrast and fluorescence microscopy images of polymer surfaces after incubation with HL-60 cells for 24 h. On the PMBH surface, almost all of the adherent cells were stained with calcein (green image) and keep their spherical shape. On the other hand, some of the adherent cells on PBH were stained with EthD-1 (red image) and were deflated. The percentage of live cells attached to the polymer surface is summarized in Figure 11. On the PMBH surface, more than 80% of the cells were alive. However, about 50% of the cells that adhered to PBH were dead. The biological

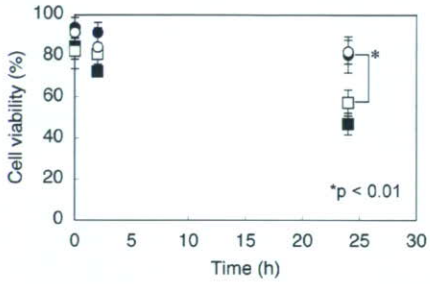

Figure 11. Time-dependence of viability of adherent cells on polymer surfaces. Open circle: PMBH2, filled circle: PMBH5, open square: PBH2, filled square: PBH5.

functions of HL-60 cells in contact with polymer surfaces were retained.

When we previously measured the cytoplasmic free calcium concentration in platelets in contact with an MPC polymer surface, the calcium concentration was unaffected and stayed at its native value (*34*). Moreover, the inflammatory response of differentiated HL-60 cells that adhered to the MPC polymer surface was investigated by the determination of IL-1β mRNA (*41*). While the expression of IL-1β mRNA from adherent cells was observed on conventional polymer materials, secreted mRNA was not observed on the MPC polymer surface, which has an MPC unit mole fraction of more than 0.2. MPC units on a polymer surface probably act to maintain the native condition of attached cells.

Coculture of HL-60 and HeLa Cells on a Polymer Surface. To clarify the possibility of using a polymer surface to recognize specific cells with cell-surface tags, the coculture of ManLev-treated HL-60 cells with native HeLa cells was examined. HeLa cells are a typical cancer cell and nonspecifically adhere to a conventional polymer surface through cell-binding proteins adsorbed on the surface. Figure 12 shows phase-contrast and fluorescence microscopy images of polymer surfaces after the coculture experiment. Cell adhesion was completely suppressed on the PMB surface. On the other hand, both HL-60 and HeLa cells were observed on PBH. HL-60 cells selectively attached to PMBH, while HeLa cells did not. The adhesion of HeLa to a polymer surface is closely associated with the adsorption of cell-binding proteins, such as fibronectin, fibrinogen, and vitronectin, on the surface because these proteins have an RGD binding site for integrin of the cell membrane (*45*). On PMBH, the

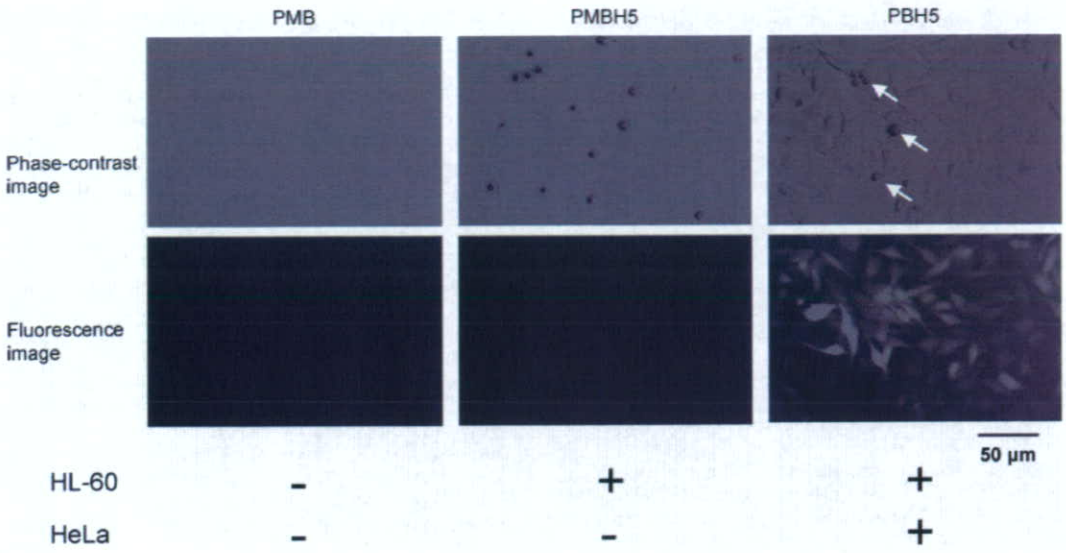

Figure 12. Phase-contrast and fluorescence micrographs of polymer surfaces after the coculture experiment. White arrows represent HL-60.

adhesion of HeLa cells was reduced due to fibronectin-resistance, as shown in Figure 9. It has been previously reported that MPC polymer can nonspecifically reduce plasma protein adsorption (*46*). The nonfouling property of the MPC polymer surface is quite important for achieving specific interaction with a cell.

These results indicate that cell-surface recognition by a polymer surface is evident in both single- and two-cell systems. Such recognition on an MPC polymer surface was effective in a multiple-cell system because the MPC polymer surface rejects the adhesion of cells without tags. Moreover, the control of cell attachment can be applied to a wide variety cells because the expression of unnatural carbohydrates on cell surfaces has been observed on various types of cells (*21*).

CONCLUSION

The present work describes a new cell-recognition surface that works through the coupling of ketone groups on the cell membrane with hydrazide groups on the phosphorylcholine polymer. This cell attachment was specific, and cells were recovered by the depletion of cell-surface tags. On a phosphorylcholine polymer surface, cell viability was effectively retained. Moreover, controlled cell attachment was not affected by the presence of serum protein. The control of cell attachment in a multicellular system was also demonstrated.

Prescher and co-workers recently reported that cell-surface modification with monosaccharides could be applied in a living animal (*47*). Tagging of cancer cells in vivo may be possible through cell-surface engineering because cancer cells have a higher metabolic flux than normal cells (*26*). It has been reported that nanoparticles coated with MPC polymer were not recognized by macrophages (*48*), and they could be used as long-term circulating drug carriers in the blood stream. It may be possible to develop a novel drug targeting system if the functionalities for recognizing cell-surface tags of a cancer cell or a specific tissue can be put on nanoparticles. Moreover, various types of polymer materials using MPC, such as films (*49*), fibers (*50*), nanoparticles (*51*), and micelles (*52*), can be prepared. Cell-surface recognition with MPC polymer promises to be an important technology in drug delivery and bioreactor systems.

ACKNOWLEDGMENT

We thank the New Energy and Industrial Technology Development Organization (NEDO) Japan (Industrial Technology Research Grant in '04, 04A02025) for financial support.

LITERATURE CITED

(1) Ratner, B. D. (1996) The engineering of biomaterials exhibiting recognition and specificity. *J. Mol. Recognit. 9*, 617–625.
(2) Ratner, B. D. (1993) New ideas in biomaterials science—a path to engineered biomaterials. *J. Biomed. Mater. Res. 27*, 837–850.
(3) Lee, J. H., and Lee, H. B. (1993) A wettability gradient as a tool to study protein adsorption and cell adhesion on polymer surfaces. *J. Biomater. Sci. Polym. Ed. 4*, 467–481.
(4) Mrksich, M., Chen, C. S., Xia, Y., Dike, L. E., Ingber, D. E., and Whitesides, G. M. (1996) Controlling cell attachment on contoured surfaces with self-assembled monolayers of alkanethiolates on gold. *Proc. Natl. Acad. Sci. 93*, 10775–10778.
(5) Ito, Y. (1999) Surface micropatterning to regulate cell functions. *Biomaterials 20*, 2333–2342.
(6) Massia, S. P., and Hubbell, J. A. (1991) Human endothelial cell interactions with surface-coupled adhesion peptides on a nonadhesive glass substrate and two polymeric biomaterials. *J. Biomed. Mater. Res. 25*, 223–242.
(7) Lin, H. B., Garcia-Echeverria, C., Asakura, S., Sun, W., Mosher D. F., and Cooper, S. (1992) Endothelial cell adhesion on polyurethanes containing covalently attached RGD-peptides. *Biomaterials 13*, 905–914.
(8) Sugawara, T., and Matsuda, T. (1995) Photochemical surface derivatization of a peptide containing Arg-Gly-Asp (RGD). *J. Biomed. Mater. Res. 29*, 1047–1052.
(9) Shakesheff, K., Cannizzaro, S., and Langer R. (1998) Creating biomimetic micro-environments with synthetic polymer-peptide hybrid molecules. *J. Biomater. Sci. Polym. Ed. 9*, 507–518.
(10) VandeVondele, S., Voros, J., and Hubbell, J. A. (2003) RGD-grafted poly-L-lysine-graft-(poly(ethyleneglycol)) copolymers block non-specific protein adsorption while promoting cell adhesion. *Biotechnol. Bioeng. 82*, 784–90.

(11) Murphy, W. L., Mercurius, K. O., Koide, S., and Mrksich, M. (2004) Substrates for cell adhesion prepared via active site-directed immobilization of a protein domain. *Langmuir 20*, 1026−1030.

(12) Hersel, U., Dahmen, C., and Kessler, H. (2003) RGD modified polymers: biomaterials for stimulated cell adhesion and beyond. *Biomaterials 24*, 4385−4415.

(13) Massia, S. P., and Hubbell, J. A. (1991) An RGD spacing of 440 nm is sufficient for integrin alpha V beta 3-mediated fibroblast spreading and 140 nm for focal contact and stress fiber formation. *J. Cell Biol. 114*, 1089−1100.

(14) Kato, K., Umezawa, K., Funeriu D. P., Miyake, M., Miyake, J., and Nagamune, T. (2003) Immobilized culture of nonadherent cells on an oleyl poly(ethylene glycol) ether-modified surface. *Biotechniques 35*, 1014−1021.

(15) Fujimoto, K. (2002) Supramolecular approaches for cellular modulation. *Supramolecular Design for Biological Applications* (Yui, N., Ed.) pp 343−369, Chapter 17, CRC Press, New York.

(16) Armstrong, J. K., Meiselman, H. J., and Fisher, T. C. (1997) Covalent binding of poly(ethylene glycol) (PEG) to the surface of red blood cells inhibits aggregation and reduces low shear blood viscosity. *Am. J. Hematol. 56*, 26−28.

(17) Panza, J. L., Wagner, W. R., Rilo, H. L., Rao, R. H., Beckman, E. J., and Russell, A. J. (2000) Treatment of rat pancreatic islets with reactive PEG. *Biomaterials 21*, 1155−1164.

(18) Fujimoto, K., Ito. K., and Kawaguchi, H. (1998) Modification and functionalization of cell surface by polymer chains with cell-adhesive ligands. *Abstr. Pap. Am. Chem. Soc. 216*, 318.

(19) Dwek, R. A. (1996) Glycobiology: Toward Understanding the Function of Sugars. *Chem. Rev. 96*, 683−720.

(20) Mahal, L. K., Yarema, K. J., and Bertozzi, C. R. (1997) Engineering chemical reactivity on cell surfaces through oligosaccharide biosynthesis. *Science 276*, 1125−1128.

(21) Yarema, K. J., Mahal, L. K., Bruehl, R. E., Rodriguez, E. C., and Bertozzi, C. R. (1998) Metabolic delivery of ketone groups to sialic acid residues. Application To cell surface glycoform engineering. *J. Biol. Chem. 273*, 31168−31179.

(22) Saxon, E., and Bertozzi, C. R. (2000) Cell surface engineering by a modified Staudinger reaction. *Science 287*, 2007−2010.

(23) Yarema, K. J., and Bertozzi, C. R. (2001) Characterizing glycosylation pathways. *Genome Biol. 2*, REVIEWS0004.

(24) Lemieux, G. A., Yarema, K. J., Jacobs, C. L., and Bertozzi, C. R. (1999) Exploiting differences in sialoside expression for selective targeting of MRI contrast reagents. *J. Am. Chem. Soc. 121*, 4278−4279.

(25) Lee, J. H., Baker, T. J., Mahal, L. K., Zabner, J., Bertozzi, C. R., Wiemer, D. F., and Welsh, M. J. (1999) Engineering novel cell surface receptors for virus-mediated gene transfer. *J. Biol. Chem. 274*, 21878−21884.

(26) Keppler, O. T., Horstkorte, R., Pawlita, M., Schmidt, C., and Reutter, W. (2001) Biochemical engineering of the N-acyl side chain of sialic acid: biological implications. *Glycobiology 11*, 11R−18R.

(27) Sadamoto, R., Niikura, K., Sears, P. S., Liu, H., Wong, C. H., Suksomcheep, A., Tomita, F., Monde, K., and Nishimura, S. (2002) Cell-wall engineering of living bacteria. S. *J. Am. Chem. Soc. 124*, 9018−9019.

(28) Sadamoto, R., Niikura, K., Ueda, T., Monde, K., Fukuhara, N., and Nishimura, S. (2004) Control of bacteria adhesion by cell-wall engineering. *J. Am. Chem. Soc. 126*, 3755−3761.

(29) Datta, D., Wang, P., Carrico, I. S., Mayo, S. L., and Tirrell, D. A. (2002) A designed phenylalanyl-tRNA synthetase variant allows efficient in vivo incorporation of aryl ketone functionality into proteins. *J. Am. Chem. Soc. 124*, 5652−5653.

(30) Kirshenbaum, K., Carrico, I. S., and Tirrell, D. A. (2002) Biosynthesis of proteins incorporating a versatile set of phenylalanine analogues. *ChemBioChem 3*, 235−237.

(31) Kiick, K. L., Saxon, E., Tirrell, D. A., and Bertozzi, C. R. (2002) Incorporation of azides into recombinant proteins for chemoselective modification by the Staudinger ligation. *Proc. Natl. Acad. Sci. U.S.A. 99*, 19−24.

(32) Link, A. J., and Tirrell, D. A. (2003) Cell Surface Labeling of *Escherichia coli* via Copper(I)-Catalyzed [3 + 2] Cycloaddition. *J. Am. Chem. Soc. 125*, 11164−11165.

(33) Link, A. J., Vink, M. K. S., and Tirrell, D. A. (2004) Presentation and Detection of Azide Functionality in Bacterial Cell Surface Proteins. *J. Am. Chem. Soc. 126*, 10598−10602.

(34) Iwasaki, Y., Mikami, A., Kurita, K., Yui, N., Ishihara, K., and Nakabayashi, N. (1997) Reduction of surface-induced platelet activation on phospholipid polymer. *J. Biomed. Mater. Res. 36*, 508−515.

(35) Iwasaki, Y., Sawada, S., Nakabayashi, N., Khang, G., Lee, H. B., and Ishihara, K. (1999) The effect of the chemical structure of the phospholipid polymer on fibronectin adsorption and fibroblast adhesion on the gradient phospholipid surface. *Biomaterials 20*, 2185−2191.

(36) Ishihara, K., Ishikawa, E., Iwasaki, Y., and Nakabayashi, N. (1999) Inhibition of fibroblast cell adhesion on substrate by coating with 2-methacryloyloxyethyl phosphorylcholine polymers. *J. Biomater. Sci. Polym. Ed. 10*, 1047−1061.

(37) Iwasaki, Y., Nakabayashi, N., and Ishihara, K. (2001) Preservation of platelet function on 2-methacryloyloxyethyl phosphorylcholine-graft polymer as compared to various water-soluble graft polymers *J. Biomed. Mater. Res. 57*, 72−78.

(38) Ishihara, K., Oshida, H., Endo, Y., Ueda. T., Watanabe, A., and Nakabayashi, N. (1992) Hemocompatibility of human whole blood on polymers with a phospholipid polar group and its mechanism. *J. Biomed. Mater. Res. 26*, 1543−1552.

(39) Ishihara, K., Nomura, H., Mihara, T., Kurita, K., Iwasaki. Y., and Nakabayashi, N. (1998) Why do phospholipid polymers reduce protein adsorption? *J. Biomed. Mater. Res. 39*, 323−330.

(40) Iwasaki, Y., Sawada, S., Ishihara, K., Khang, G., and Lee, H. B. (2002) Reduction of surface-induced inflammatory reaction on PLGA/MPC polymer blend. *Biomaterials 23*, 3897−3903.

(41) Sawada, S., Sakaki, S., Iwasaki, Y., Nakabayashi, N., and Ishihara, K. (2003) Suppression of the inflammatory response from adherent cells on phospholipid polymers. *J. Biomed. Mater. Res. 64A*, 411−416.

(42) Ishihara, K., Ueda, T., and Nakabayashi, N. (1990) Preparation of phospholipid polymers and their properties as polymer hydrogel membrane. *Polym. J. 22*, *355−360.*

(43) Saxon, E., Luchansky, S. J., Hang, H. C., Yu, C., Lee, S. C., and Bertozzi, C. R. (2002) Investigating cellular metabolism of synthetic azidosugars with the Staudinger ligation. *J. Am. Chem. Sci. 124*, 14893−14902.

(44) Baszkin, A., and Lyman, D. J. (1980) The interaction of plasma proteins with polymers. I. Relationship between polymer surface energy and protein adsorption/desorption. *J. Biomed. Mater. Res. 14*, 393−403.

(45) Hirano, Y., Okuno, M., Hayashi, T., Goto, K., and Nakajima, A. (1993) Cell-attachment activities of surface immobilized oligopeptides RGD, RGDS, RGDV, RGDT, and YIGSR toward five cell lines. *J. Biomater. Sci. Polym. Ed. 4*, 235−243.

(46) Ishihara, K., Ziats, N. P., Tierney, B. P., Nakabayashi, N., and Anderson, J. M. (1991) Protein adsorption from human plasma is reduced on phospholipid polymers. *J. Biomed. Mater. Res. 25*, 1397−1407.

(47) Prescher, J. A., Duhe, D. H., and Bertozzi, C. R. (2004) Chemical remodelling of cell surfaces in living animals. *Nature 430*, 873−877.

(48) Konno, T., and Ishihara K. (2001) Blood Compatible Nanoparticles Immobilized with 2- Methacryloyloxyethyl Phosphorylcholine Polymer. *Trans. Mater. Res. Soc. Jpn. 26*, 897−900.

(49) Iwasaki, Y., Uchiyama, S., Kurita, K., Morimoto, N., and Nakabayashi, N. (2002) A nonthrombogenic gas-permeable membrane composed of a phospholipid polymer skin film

adhered to a polyethylene porous membrane. *Biomaterials 23*, 3421−3427.
(50) Hasegawa, T., Iwasaki, Y., and Ishihara, K. (2001) Preparation and performance of protein-adsorption-resistant asymmetric porous membrane composed of polysulfone/phospholipid polymer blend. *Biomaterials 22*, 243−51.
(51) Konno, T., Kurita, K., Iwasaki, Y., Nakabayashi, N., and Ishihara, K. (2001) Preparation of nanoparticles composed with bioinspired 2-methacryloyloxyethyl phosphorylcholine polymer. *Biomaterials 22*, 1883−1889.
(52) Ishihara, K., Iwasaki, Y., and Nakabayashi, N. (1999) Polymeric lipid nanosphere consisting of water-soluble poly(2-methacryloyloxyethyl phosphorylcholine-*co*-*n*-butyl methacrylate). *Polym. J. 31*, 1231−1236.

BC049707R

Summary: Polymerizable nanogels were prepared by self-assembly of cholesteryl group-bearing pullulan (CHP) with methacryloyl groups (CHPMA). The CHPMA nanogel was polymerized with 2-methacryloyloxyethyl phosphorylcholine (MPC) by radical polymerization in dilute aqueous solution. The solution properties of the polymers in water were investigated by TEM, SEC-MALS, and fluorescence quenching technique. Monodispersed hybrid nanogels of CHPMA-MPC (CM nanogels) (25–30 nm in radius of gyration) were obtained by using CHPMA nanogel as a seed-nanogel. CM nanogels have a dual cross-linking structure that is physically cross-linked with the cholesteryl groups and chemically cross-linked with the MPC polymer chains. CM nanogels trap heat-denatured carbonic anhydrase B (CAB) and prevent their aggregations. The nanogels maintained the ability of trapping and releasing enzymes by host-guest interaction of cholesteryl group and cyclodextrin.

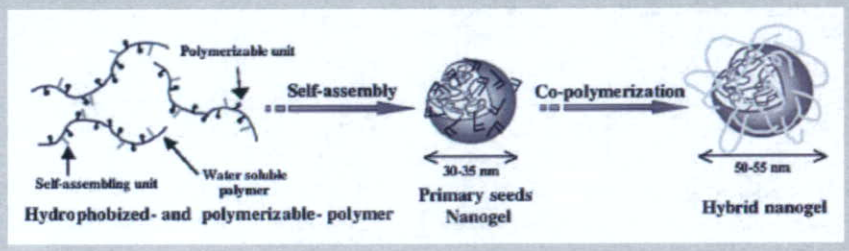

Schematic illustration of hybrid nanogel preparation.

Hybrid Nanogels with Physical and Chemical Cross-Linking Structures as Nanocarriers[a]

Nobuyuki Morimoto,[1] *Takao Endo,*[2] *Michiko Ohtomi,*[2] *Yasuhiko Iwasaki,*[1] *Kazunari Akiyoshi**[1,3]

[1] Institute of Biomaterials and Bioengineering, Tokyo Medical and Dental University, 2-3-10, Kanda-surugadai, Chiyoda-ku, Tokyo 101-0062, Japan
[2] Department of Biomolecular Science, Faculty of Science, Toho University, 2-2-1 Miyama, Funabashi-shi, Chiba 274-8510, Japan
[3] Center of Excellence Program for Frontier Research on Molecular Destruction and Reconstruction of Tooth and Bone, Tokyo Medical and Dental University, Tokyo, Japan
Fax: (+81) 3-5280-8027; E-mail: akiyoshi.org@tmd.ac.jp

Received: March 11, 2005; Revised: June 4, 2005; Accepted: June 9, 2005; DOI: 10.1002/mabi.200500051

Keywords: drug delivery systems; microgels; nanoparticles; polysaccharides; protein

Introduction

Polymer hydrogels have been widely used as functional materials for biotechnological and biomedical applications.[1] Sub-micron-sized (<100 nm) polymer hydrogel particles (nanogels) have attracted growing interest due to recent developments in nanotechnology. Compared to other nanoparticles that are mainly used for their unique surface properties, nanogels are expected to exhibit additional properties to trap various substances such as drugs and biomacromolecules inside the gel. Therefore, there has been interest in the application of nanogels in drug delivery systems, such as protein delivery and gene delivery.[2] In general, chemically cross-linked nanogels are synthesized by microemulsion polymerization,[3] a cross-linking reaction of intra-associated polymer molecules,[4] and chemical cross-linking of core-shell type micelles.[5]

We reported a novel method for the self-assembly of physically cross-linked nanogels by the controlled association of the cholesteryl group-bearing pullulan (CHP).[6] The CHP molecules associated in dilute aqueous solution and formed monodispersed nanogels in which the associations of hydrophobic groups provided physical cross-linking points.

[a] Supporting information for this article is available at the bottom of the article's abstract page, which can be accessed from the journal's homepage at http://www.mbs-journal.de, or from the author.

 DOI: 10.1002/mabi.200500051

The size, density, and number of cross-linking domains of these nanoparticles are regulated by the number of hydrophobic groups as well as by their structures.[6c] An interesting property of CHP nanogels is their ability to form complexes with various soluble proteins in water.[7] The complexed protein in a nanogel can be released by interaction with other proteins[7] or by the addition of β-cyclodextrin (β-CD), which dissociates physical cross-links within the CHP nanogel.[8] The nanogels can be used as drug-carrier systems in medicine[9] and as artificial molecular chaperones in biotechnology.[8,10] We are able to develop tailor-made functional nanogels to create novel nanobiomaterials (nanogel engineering) by the self-assembly of functional associating polymers as building blocks. Various nanogels were obtained by the self-assembly of cholesteryl-bearing poly(amino acids),[11] an alkyl group-modified poly(*N*-isopropylacrylamide)-CHP mixture,[12] and a spiropyrane-modified pullulan,[13] deoxycholic acid-modified chitosan,[14] bile acid-bearing dextran,[15] and synthetic polyelectrolytes with hydrophobic groups.[16]

Here, we report a new method for the preparation of synthetic polymer-polysaccharide hybrid nanogels by using a polymerizable nanogel as a seed nanoparticle. A self-assembled nanogel containing polymerizable groups was prepared as the key building block. Monodispersed hybrid nanogels with physical and chemical cross-linking structures were then constructed by the copolymerization of nanogels with appropriate water-soluble monomers under dilute conditions. We have already reported that CHP nanogels were useful as nanocarriers. CHP nanogels were complexed with various antitumor drugs such as adriamycin[17] and neocarzinostatin chromophores[18] as well as with proteins such as insulin and tumor antigens.[9b,c] However, the stability of CHP nanogels, especially in the bloodstream, is not high due to the physical cross-linking structure. In this study, to overcome this problem and also to develop stealth-type nanogels, we designed hybrid nanogels composed of polysaccharide–2-methacryloyloxyethyl phosphorylcholine (MPC). MPC polymers exhibit high water solubility and resist nonspecific protein adsorption and cell adhesion.[19] In fact, polymer nanoparticles coated with MPC polymers were not even recognized by macrophages.[20] The colloidal stability of the nanogels can also be improved by the conjugation of MPC polymers with CHP nanogels as well as chemical cross-links with MPC polymers inside the nanogels. CHP-MPC hybrid nanogels can be useful in drug delivery systems.

Experimental Part

Materials

Cholesteryl group-bearing pullulan was synthesized as reported previously.[6a] Pullulan was used with an average molecular weight ($\overline{M}_w$) of 1.0×10^5. The degree of substitution of the hydrophobic groups in CHP was approximately 1.2 per 100 glucose units. MPC was also synthesized as reported previously.[17a] 2,2′-Azobis[2-(2-imidazolin-2-yl) propane] (VA-044) was donated by WAKO Chemical Co. Ltd. (Tokyo, Japan). Glycidyl methacrylate (GMA) was purchased from Nakalai Tesque (Tokyo, Japan) and distilled under reduced pressure; the fraction of bp 48 °C/3.5 mmHg was used. β-CD and other reagents were purchased from WAKO and used without further purification.

Synthesis of Methacryloyl Group-Bearing CHP (CHPMA)

Cholesteryl group-bearing pullulan with methacryloyl groups (CHPMA) was synthesized by the same procedures as reported previously.[21] CHP was used after being dried in vacuo at 70 °C for 3 d. CHP (1.5 g) was dissolved in DMSO (30 mL), and then 4-dimethylamino pyridine (DMAP, 0.49 g) and GMA (0.53 mL) were added. The reaction was kept at room temperature for 24 h. The reaction was stopped by adding HCl, after which the product was isolated after extensive dialysis and freeze-drying. Quantitative determination of the methacrylate was determined by measuring the ratio between the average values of the double bond proton integrals of the ^{1}H NMR spectra.

Preparation of MPC Polymer Modified CHP Nanogel (CM nanogel)

An MPC polymer modified CHP (CM nanogel) was prepared by free radical polymerization in a diluted monomer solution of water. First, CHPMA nanogels were prepared as seed nanoparticles. CHPMA (200 mg) was dissolved in distilled water (final concentration: 1.0 mg · mL^{-1}) and sonicated by a probe-type sonicator at 40 W for 15 min. The MPC monomer solution (10 mg · mL^{-1}) was then added as required at each condition. The MPC monomer was added in a molar ratio of 10 or 100 per methacryloyl group in CHPMA. 2,2′-Azobis[2-(2-imidazolin-2-yl) propane] (VA-044) was added as an initiator of radical polymerization with a concentration of 0.5 mol-% against monomers. After argon bubbling to remove oxygen, the solution was polymerized at 50 °C for 5 h with Ar purging and stirring under refluxing. The solution was dialyzed against water for 7 d, concentrated with ultrafiltration, and then reprecipitated with ethanol and dried in vacuo (Figure 1). The introduction of the MPC units and the molecular weight ($\overline{M}_w$) of the prepared CM were estimated by ^{1}H NMR measurements (see *Supporting Information*).

Size-Exclusion Chromatography (SEC)–Multi-Angle Laser Light Scattering (MALS) Measurements

Size-exclusion chromatography (SEC) was performed on a chromatography system (Tosoh Co. Ltd., Tokyo, Japan) connected to an MALS detector (DAWN DSP, Wyatt Technology, Santa Barbara, CA) in the presence or absence of β-CD (10 mM). As the columns, TSK gel G4000 SW (Tosoh) was used for CHPMA (Figure 2) and CM6 nanogels, and OHpak SB806M HQ (Showa Denko Co. Ltd., Tokyo, Japan) was used for the CM14 nanogels. The eluting buffer was 50 mM NaCl in

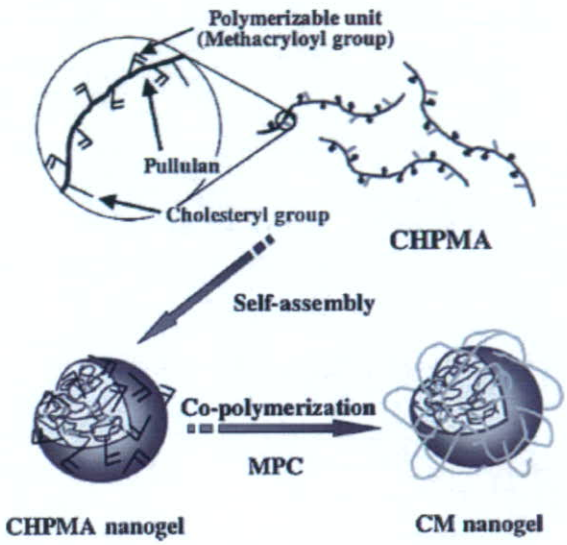

Figure 1. Schematic illustration of CM nanogel preparation.

H_2O and the flow rate was 0.5 mL · min^{-1}. The molecular weight ($\bar{M}_w$), polydispersity index ($\bar{M}_w/\bar{M}_n$), and the z-average root-mean-square radius of gyration (R_g) were determined using ASTRA software based on Zimm's equation. The refractive index increment (dn/dc) was determined by Optilab DSP (Wyatt Technology, Santa Barbara, CA). The values of dn/dc were 0.143 for CHPMA, and 0.127 for the CM nanogels.

Fluorescence Quenching Technique

The aggregation number of an associating cholesterol domain was estimated by using the steady-state quenching technique.[6b] Fluorescence spectra were recorded on a fluorescence spectrophotometer (FP-750, Jasco, Tokyo, Japan). The data were fitted in the quenching kinetics,

$$\ln(I_0/I) = [Q]/[M] \quad (1)$$

where I and I_0 are the fluorescence intensity in the presence or absence of a quencher, $[Q]$ is the bulk concentration of the quencher, and $[M]$ is the concentration of the polymer self-aggregate. The plot of $\ln(I_0/I)$ against the quencher concentration gives a straight line, the slope of which corresponds to $[M]^{-1}$. Thus, the aggregation number, N_{sample}, can be calculated as

$$N_{sample} = [\text{cholesteryl group}]/[M] \quad (2)$$

A stock solution of pyrene in ethanol (1×10^{-4} M) was added to a vial, and ethanol was evaporated by flushing gaseous nitrogen to form a thin film sample at the bottom of the vial. The CM nanogel suspension was added to the thin film, and the resulting mixture was stirred overnight. The final concentration of pyrene in the vial was 1×10^{-6} M. An aqueous solution of cetylpyridinium chloride was added just before the measurements. Pyrene was excited at 339 nm.

Transmission Electron Micrograph (TEM) Observation

TEM was performed on an H-600 (Hitachi, Tokyo, Japan) at an accelerating voltage of 100 V. For the CM nanogels, specimens were prepared by dropping 10 μL of dilute polymer solution (0.2 mg · mL^{-1}) on a grid and staining with 2% uranyl acetate.

Refolding of Heat-Denatured Carbonic Anhydrase B (CAB)

The procedure of heat-induced aggregation and the refolding of CAB was used according to the method described previously.[8] A CAB (15 μg · mL^{-1}) solution of Tris-sulfate buffer (pH 7.5, 50 mM) was denatured in the presence or absence of nanogels (4.8 mg · mL^{-1}) at 70 °C for 10 min. After the solution was cooled to 20 °C, β-CD (10 mM) was added and the mixture was kept for 2 h. A dry acetonitrile solution of *p*-nitrophenyl acetate (10 mM) was added to the sample solution. The recovery of enzyme activity was monitored as the *p*-nitrophenolate concentration by the absorbance of 400 nm as a function of time. The yield of reactivated CAB was determined by comparison with the initial rate of *p*-nitrophenyl acetate hydrolysis by the native enzyme at the same concentration.

Results and Discussion

Preparation of Polymerizable Nanogels and Hybrid Nanogels

Nanogels containing methacryloyl groups were designed as polymerizable units. CHP reacted with glycidyl methacrylate (GMA) in the presence of 4-dimethylamino pyridine (DMAP) in DMSO.[21] The degree of substitution of

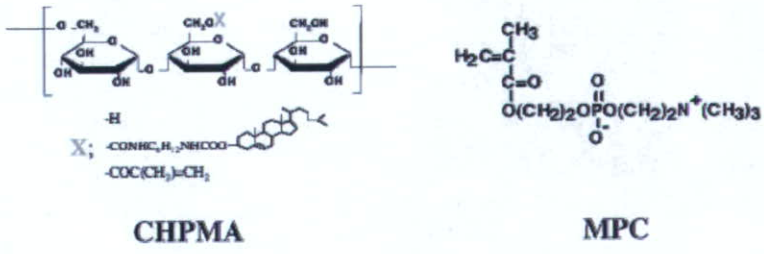

Figure 2. Chemical structure of CHPMA and MPC.

Table 1. Characterization of nanogels.

Abb.	Molar ratio of methacrylates[a)]	$\bar{M}_w$ ($\times 10^5$)	$\bar{M}_w/\bar{M}_n$	MPC units in nanogel	R_g	ϕ_g	Aggregation number of hydrophobe
				wt.-%	nm	%	
CM6	6.2	6.0	1.18	37.9	28.4 ± 3.0	1.0	3.5 ± 0.6
CM14	14.3	10.1	1.08	60.8	26.6 ± 1.0	2.1	3.4 ± 0.4
CHPMA	–	4.5	1.20	0	17.2 ± 3.2	3.5	3.6 ± 0.5

[a)] Number of MPC units per methacrylate in CHPMA.

methacryloyl groups was calculated by the ratio between the peak of the double bond protons (δ 5.65–6.15 ppm) and that of the glucose unit *1H* protons (δ 4.60–4.75 and δ 4.90–5.05 ppm) in ^{1}H NMR spectrum. Approximately six methacryloyl groups per 100 glucose units of pullulan were introduced to CHP. Similar to CHP, the methacryloyl groups-bearing CHP (CHPMA) formed nanogels by self-assembly in water. The radius of gyration of the nanogels was 17.2 ± 3.2 nm, and the association number of CHPMA per nanogel was approximately 4.1 as estimated by the SEC-MALS method (Table 1). The number of polymerizable groups per nanogel was calculated from the association number; the degree of methacryloyl group substitution was about 160.

The polymerizable nanogels were considered to be multimacromonomers. CHPMA can be copolymerized with a variety of water-soluble monomers. As a comonomer, we selected hydrophilic 2-methacryloyloxyethyl phosphorylcholine (MPC). Free radical polymerizations in water were performed at 50 °C for 5 h in the presence of CHPMA nanogels (final concentration: 1.0 mg · mL^{-1}) and MPC (final concentraion: 1.1 or 11.0 mg · mL^{-1}) using 2, 2′-azobis [2-(2-imidazolin-2-yl) propane] (VA-044) as an initiator. Based on an analysis of ^{1}H NMR, all of the methacryloyl groups in CHPMA were reacted under these conditions. The degree of polymerization of MPC was calculated by the ratio between the peak of the choline group protons (δ 3.18–3.30 ppm) and that of the glucose unit *1H* protons (δ 4.60–4.75 and δ 4.90–5.05 ppm) in ^{1}H NMR spectrum. In the copolymers, there were 6.1 (CM6) and 14.3 (CM14) MPC units per methacryloyl group in CHPMA.

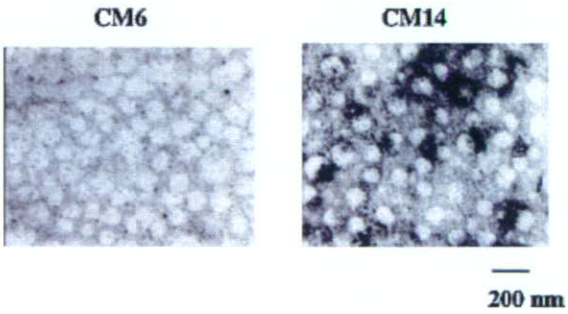

Figure 3. TEM images of CM nanogels.

Characterization of Hybrid Nanogels

The solution properties of the CMs in water were investigated. The samples were prepared by dispersing freeze-dried powders of the polymers in water followed by sonication for 15 min. TEM images showed that the self-assemblies of the CMs were monodispersed spherical nanoparticles (Figure 3). The radius of the CM6 and CM14 nanoparticles calculated from TEM images were 69 ± 13 nm and 71 ± 8 nm, respectively. Figure 4(a) and (c) are gel chromatograms of the CM nanogels. They were monodispersed and had limited size distributions. Because the cross-linking reactions between nanogels are suppressed in a dilute aqueous solution, it was possible to prepare a hybrid nanogel composed of both polysaccharides and MPC polymers. In the presence of higher concentrations of CHP nanogels and MPC, macrogels formed after polymerization.[21]

The molecular weights and sizes of the nanogels were obtained by SEC-MALS (Table 1). The average polymer density ($\emptyset_g$) in one nanoparticle was calculated from R_g and $\bar{M}_w$ of each nanogel by using Equation (3)[6b]

$$\emptyset_g = \bar{M}_w/N_A \times (4/3\pi R_g^3)^{-1} \quad (3)$$

where N_A is Avogadro's number. The densities of the CHPMA, CM6, and CM14 nanogels were 0.035, 0.010, and 0.021 g · mL^{-1}, respectively. These values correspond to 3.5, 1.0, and 2.1 wt.-% hydrogels. The methacryloyl groups of CHPMA were located both inside and outside the nanogels. After polymerization, MPC polymers probably locate on the surface and also inside the nanogels. The increases in the sizes and densities of the nanogels after polymerization may be due to their swelling by the introduction of hydrophilic MPC chains and also due to covering the polysaccharide core nanogel by MPC polymer chains. The water solubility and colloidal stability of the CHP-MPC hybrid nanogels increased compared with that of the CHP nanogels. No precipitation of CHP-MPC nanogels was observed in water at 20 °C for at least three months.

The aggregation numbers of the cholesteryl groups in the CM nanogels were estimated by fluorescence quenching technique as previously reported.[6b] The value of I_3/I_1, the ratio of fluorescence intensity of pyrene at 384 to that at 377 nm, can be used to examine the microenvironment of the excited pyrene. The value increases with an increase in

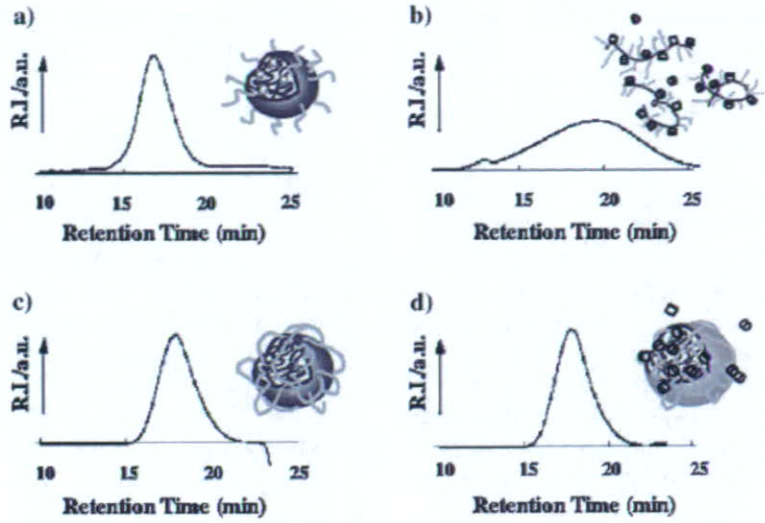

Figure 4. Chromatogram of SEC-MALS (RI response) and schematic illustration of each sample; (a) CM6 nanogel, (b) CM6 nanogel + 10 mM β-CD, (c) CM14 nanogel, and (d) CM14 nanogel + 10 mM β-CD. The eluting buffer was 50 mM NaCl in H_2O and the flow rate was 0.5 mL · min^{-1}.

the hydrophobicity of the microenvironment (0.53 in water). The values in the CM nanogels (CM6: 0.96, CM14: 0.92) were similar to those in the CHPMA nanogels (0.99). The results indicate that pyrene was trapped in the hydrophobic microdomains in the nanogels. The fluorescence quenching experiment was performed using pyrene as a fluorescence probe and cetylpyridinium chloride as a quencher (see also *Supporting Information*). The association numbers of the cholesteryl groups in each nanogel did not change at all after polymerization [3.6 ± 0.5 (CHPMA), 3.5 ± 0.6 (CM6), and 3.4 ± 0.4 (CM14)]. Associations of cholesteryl groups in one domain are limited by steric hindrance of the polymer chain. One nanoparticle of both CM6 and CM14 consists of approximately 30 cholesteryl groups. Therefore, there are about eight cross-linking points in a CM nanogel. These nanoparticles are considered to be microscopic hydrogels (nanogels) in which the associations of hydrophobic groups provide cross-linking points in the polymer network. The domains of the cholesteryl groups remained as physical cross-linking points even after polymerization.

Interaction of Hybrid Nanogels with Cyclodextrin

A unique property of self-assembled nanogels is that their generation and collapse can be dynamically controlled by host-guest interaction of their cholesteryl groups with cyclodextrin.[22] Since the cholesteryl group is a suitable guest for β-CD,[23] the CHP nanogels dissociated upon complexation with β-CD to yield a dissociated CHP-CD complex. The interaction of the CM nanogels with β-CD was investigated to determine the cross-linking structure of the CM nanogels. When CHP nanogels were added to β-CD, the cholesteryl groups and β-CD formed an inclusion complex. Because of the disappearance of the physical cross-linking points, the CHP nanogels dissociated into single macromolecules. As shown in Figure 4(b), the CM6 nanogels dissociated in the presence of β-CD in a manner similar to the CHP nanogels. In this case, the buffer containing β-CD was used as an eluent. The peak is attributed to the CM6-CD complex. Based on SEC-MALS, the molecular weight of the CM6-CD complex was estimated to be 2.1×10^5 ($\overline{M}_w/\overline{M}_n = 1.4$). This value agrees with the molecular weight (1.9×10^5) of the CM6 macromolecule calculated from the data of ^{1}H NMR analysis. CM nanogels (both CM6 and CM14 nanogels) consist of 3–4 CM macromolecules, as shown in Table 1. In CM6 nanogels, the MPC polymer chain may be too short for intermacromolecularly cross-linking, and no cross-linking or only intramacromolecular cross-linking occurred. Therefore, CM6 nanogels dissociated to each CM macromolecule.

In contrast, there was little change in the CM14 nanogels in the presence of β-CD [Figure 4(d)]. The molecular weight was 12.1×10^5 ($\overline{M}_w/\overline{M}_n = 1.1$), and R_g was 25.7 ± 2.0 nm (for CM14 nanogels: $\overline{M}_w = 10.1 \times 10^5$ and R_g = 26.6 ± 1.0 nm). The increase of the molecular weight of the CM14 nanogels in the presence of β-CD and the effective release of proteins trapped in the CM14-β-CD nanogels after addition of β-CD (discussed in the next section) suggests that β-CD interacted with the cholesteryl groups in the CM14 nanogels. CM14-β-CD complex-nanogels probably formed without the dissociation. The polymer chain in the CM14 nanogel is more densely packed than that in the CM6 nanogel. No dissociation of CM14

macromolecules by complexation with β-CD is probably due to intermacromolecular chemical cross-linking by the MPC polymer chains. The CM nanogels have a dual cross-linking structure that is physically cross-linked with the cholesteryl groups and chemically cross-linked with the MPC polymer chains.

Interaction of Hybrid Nanogels with Proteins

It is important to trap proteins in hydrogels without their aggregations and to control release of proteins in a native form for developing effective protein reservoirs in drug delivery systems and artificial molecular chaperones in biotechnology. Irreversible adsorption of proteins is sometimes unavoidable in trapping them in the hydrogels because it is generally difficult to control the mesh size of the hydrogel matrix and also the cross-linking sites. We previously reported that even denatured proteins that were trapped in the nanogels without aggregations can be refolded to intact forms after being released from the nanogels and are therefore useful as artificial chaperones[8,10] or drug carriers.[9] In this study, we investigated whether the ability to trap and release proteins by the addition of cyclodextrin (CD) remains after conjugation of the MPC polymers and chemical cross-linking. The results also provide important insights into the cross-linking structure of the nanogels.

Carbonic anhydrase B (CAB) was selected as a model enzyme. CAB aggregated and precipitated after being heated at 70 °C for 10 min. In this process, exposure of the hydrophobic surface of the heat-denatured protein results in irreversible aggregation. In the presence of hybrid nanogels, however, the solution was transparent even after heating under the same conditions. This phenomenon is caused by the complexation of the denatured CAB with the hybrid nanogels. The enzyme activity of the complex was lost by trapping denatured protein (enzyme activity of the complex, CM6 nanogels: $5.0 \pm 0.2\%$, CM14 nanogels: $5.7 \pm 0.5\%$, CHP nanogels: $5.0 \pm 0.1\%$). Hydrophobic interaction between the hydrophobic domain of the cholesteryl group in the nanogels and the exposed hydrophobic surface of the denatured protein plays an important role in the complexation. CM nanogels retain their activity of trapping heat-denatured protein.

Both complexes, CM6-CAB and CM14-CAB, were stable under this condition. No protein release from the complexes was observed at 20 °C for at least 24 h in the absence of β-CD. In the presence of β-CD, however, dissociation of the hydrophobic domain in the nanogels subsequently induced the release of the proteins as well as protein refolding, as previously reported.[8,10] Two hours after the addition of β-CD, enzyme activity recovered in both the CM6 and CM14 nanogel systems (CM6 nanogels: $66.8 \pm 1.1\%$, CM14 nanogels: $59.1 \pm 1.5\%$, CHP nanogels: $62.8 \pm 4.8\%$). The activity of the hybrid nanogels is comparable to that of the CHP nanogels. The results show that the complexation of nanogels with protein or β-CD effectively occurs even in the chemical cross-linking of the nanogels. Chemical cross-linking and surface coating by such MPC polymers did not affect the trapping and release of the protein because the hydrophobic association by physically cross-linked domains of the cholesteryl groups is important in the interaction of proteins with nanogels. In addition, the MPC polymers of the hybrid nanogels act as a suitable inert matrix for the trapped proteins due to the reduction of protein adsorption.[19] This property is essential for the application of hybrid nanogels in DDS and to artificial molecular chaperone as well as to the improved colloidal stability of nanogels by the surface coating of the MPC polymers. Based on the results, application of hybrid nanogels in DDS is now under investigation in our laboratory.

Conclusion

Monodispersed hybrid nanogels were successfully prepared by using seed-nanogels with polymerizable groups. The hybrid nanogels exhibited the ability of trapping denatured CAB and then releasing CAB in its native form. A variety of monodispersed functional nanogels can be designed by selecting various self-assembled nanogels as seeds and by selecting various functional monomers. Such hybrid nanogels are useful for applications in biotechnology and drug delivery systems.

Acknowledgements: This work was supported by a Grant-in-Aid for Scientific Research from the *Japanese Government* (No. 17300147). K. A. acknowledges the financial support from *Sekisui Chemical Co. Ltd.*

[1] [1a] J. Kopecek, *Nature* **2002**, *417*, 388; [1b] M. E. Byrne, K. Park, N. A. Peppas, *Adv. Drug Delivery Rev.* **2002**, *54*, 149.
[2] [2a] S. V. Vinogradov, T. K. Bronich, A. V. Kabanov, *Adv. Drug Delivery Rev.* **2002**, *54*, 135; [2b] K. McAllister, P. Sazani, M. Adam, M. J. Cho, M. Rubinstein, R. J. Samulski, J. M. DeSimone, *J. Am. Chem. Soc.* **2002**, *124*, 15198.
[3] D. Gan, L. A. Lyon, *J. Am. Chem. Soc.* **2001**, *123*, 7511.
[4] [4a] D. Kuckling, C. D. Vo, S. E. Wohlrab, *Langmuir* **2002**, *18*, 4263; [4b] J. Zhou, Z. Li, G. Liu, *Macromolecules* **2002**, *35*, 3690.
[5] [5a] K. B. Thumond II, T. Kowalewski, K. L. Wooley, *J. Am. Chem. Soc.* **1996**, *118*, 7239; [5b] V. Bütün, N. C. Billingham, S. P. Armes, *J. Am. Chem. Soc.* **1998**, *120*, 12135; [5c] H. Hayashi, M. Iijima, K. Kataoka, Y. Nagasaki, *Macromolecules* **2004**, *37*, 5389.
[6] [6a] K. Akiyoshi, S. Deguchi, N. Moriguchi, S. Yamaguchi, J. Sunamoto, *Macromolecules* **1993**, *26*, 3062; [6b] K. Akiyoshi, S. Deguchi, H. Tajima, T. Nishikawa, J. Sunamoto, *Macromolecules* **1997**, *30*, 857; [6c] K. Akiyoshi, J. Sunamoto, *Supramolecular Sci.* **1996**, *3*, 157.

[7] [7a] T. Nishikawa, K. Akiyoshi, J. Sunamoto, *J. Am. Chem. Soc.* **1996**, *118*, 6110; [7b] T. Nishikawa, K. Akiyoshi, J. Sunamoto, *Macromolecules* **1994**, *27*, 7654.
[8] K. Akiyoshi, Y. Sasaki, J. Sunamoto, *Bioconjugate Chem.* **1999**, *10*, 321.
[9] [9a] K. Akiyoshi, S. Kobayashi, S. Shichibe, D. Mix, M. Baudys, S. W. Kim, J. Sunamoto, *J. Controlled Release* **1998**, *54*, 313; [9b] Y. Ikuta, N. Katayama, L. Wang, T. Okugawa, Y. Takahashi, M. Schmitt, X. Gu, M. Watanabe, K. Akiyoshi, H. Nakamura, K. Kuribayashi, J. Sunamoto, H. Shiku, *Blood* **2002**, *99*, 3717; [9c] X-G. Gu, M. Schmitt, A. Hiasa, Y. Nagata, H. Ikeda, Y. Sasaki, K. Akiyoshi, J. Sunamoto, H. Nakamura, K. Kuribayashi, H. Shiku, *Cancer Res.* **1998**, *58*, 3385.
[10] Y. Nomura, M. Ikeda, N. Yamaguchi, Y. Aoyama, K. Akiyoshi, *FEBS Lett.* **2003**, *553*, 271.
[11] K. Akiyoshi, A. Ueminami, S. Kurumada, Y. Nomura, *Macromolecules* **2000**, *33*, 6752.
[12] K. Akiyoshi, E.-C. Kang, S. Kurumada, J. Sunamoto, T. Principi, F. M. Winnik, *Macromolecules* **2000**, *33*, 3244.
[13] T. Hirakura, Y. Nomura, Y. Aoyama, K. Akiyoshi, *Biomacromolecules* **2004**, *5*, 1804.
[14] [14a] K. Y. Lee, W. H. Jo, *Langmuir* **1998**, *14*, 2329; [14b] K. Y. Lee, W. H. Jo, I. C. Kwon, Y. Kim, S. Y. Jeong, *Macromolecules* **1998**, *31*, 378.
[15] M. Nichifor, A. Lopes, A. Carpov, E. Melo, *Macromolecules* **1999**, *32*, 7078.
[16] S. Yusa, M. Kamachi, Y. Morishima, *Langmuir* **1998**, *14*, 6059.
[17] K. Akiyoshi, I. Taniguchi, H. Fukui, J. Sunamoto, *Eur. J. Pharm. Biopharm.* **1996**, *42*, 286.
[18] I. Taniguchi, M. Fujiwara, K. Akiyoshi, J. Sunamoto, *Bull. Chem. Soc. Jpn.* **1998**, *71*, 2681.
[19] [19a] K. Ishihara, T. Ueda, N. Nakabayashi, *Polym. J.* **1990**, *22*, 355; [19b] K. Ishihara, H. Nomura, T. Mihara, K. Kurita, Y. Iwasaki, N. Nakabayashi, *J. Biomed. Mater. Res.* **1998**, *39*, 323; [19c] T. Konno, K. Kurita, Y. Iwasaki, N. Nakabayashi, K. Ishihara, *Biomaterials* **2001**, *22*, 1883.
[20] T. Konno, K. Ishihara, *Trans. Mater. Res. Soc. Jpn.* **2001**, *26*, 897.
[21] N. Morimoto, T. Endo, Y. Iwasaki, K. Akiyoshi, *Biomacromolecules* **2005**, *6*, 1809.
[22] K. Akiyoshi, S. Sasaki, K. Kuroda, J. Sumanoto, *Chem. Lett.* **1998**, 93.
[23] R. Breslow, B. J. Zhang, *J. Am. Chem. Soc.* **1996**, *118*, 8495.

Available online at www.sciencedirect.com
SCIENCE DIRECT®
Biomaterials 27 (2006) 2907–2915
Biomaterials
www.elsevier.com/locate/biomaterials

Leading Opinion

How useful is SBF in predicting in vivo bone bioactivity?☆

Tadashi Kokubo*, Hiroaki Takadama

Department of Biomedical Sciences, College of Life and Health Sciences, Chubu University, 1200 Matsumoto, Kasugai, Aichi 487-8501, Japan

Received 6 September 2005; accepted 13 January 2006
Available online 31 January 2006

Abstract

The bone-bonding ability of a material is often evaluated by examining the ability of apatite to form on its surface in a simulated body fluid (SBF) with ion concentrations nearly equal to those of human blood plasma. However, the validity of this method for evaluating bone-bonding ability has not been assessed systematically. Here, the history of SBF, correlation of the ability of apatite to form on various materials in SBF with their in vivo bone bioactivities, and some examples of the development of novel bioactive materials based on apatite formation in SBF are reviewed. It was concluded that examination of apatite formation on a material in SBF is useful for predicting the in vivo bone bioactivity of a material, and the number of animals used in and the duration of animal experiments can be reduced remarkably by using this method.

Keywords: Bioactivity; Bone; Hydroxyapatite; In vitro test; Osteoconduction; SBF

1. Introduction

Artificial materials implanted into bone defects are generally encapsulated by a fibrous tissue, leading to their isolation from the surrounding bone. However, in 1972, Hench et al. showed that some glasses in the Na_2O–CaO–SiO_2–P_2O_5 system, called Bioglass, spontaneously bond to living bone without the formation of surrounding fibrous tissue [1]. Since then, several types of ceramic, such as sintered hydroxyapatite [2], sintered β-tricalcium phosphate [3], apatite/β-tricalcium phosphate biphasic ceramics [4], and glass-ceramic A–W containing crystalline apatite and wollastonite [5] have been also shown to bond to living bone, and they are used clinically as important bone substitutes. However, these ceramics are not compatible mechanically to the surrounding bone. The development of bone-bonding materials with different mechanical properties is desired.

This desire leads to two questions: what type of material bonds to living bone; and are animal experiments the only one way to test for bone bonding, that is, to identify a material with in vivo bone bioactivity? In 1991, we proposed that the essential requirement for an artificial material to bond to living bone is the formation of bonelike apatite on its surface when implanted in the living body, and that this in vivo apatite formation can be reproduced in a simulated body fluid (SBF) with ion concentrations nearly equal to those of human blood plasma [6]. This means that the in vivo bone bioactivity of a material can be predicted from the apatite formation on its surface in SBF. Since then, in vivo bone bioactivity of various types of materials have been evaluated by apatite formation in SBF. However, the validity of this method has not been systematically assessed.

Here, the history of SBF, correlation of the ability of apatite to form on various materials in SBF with their in vivo bone bioactivities, and some examples of successful development of novel bioactive materials based on the apatite formation on their surfaces in SBF are reviewed.

☆*Editor's Note*: Leading Opinions: This paper is one of a newly instituted series of scientific articles that provide evidence-based scientific opinions on topical and important issues in biomaterials science. They have some features of an invited editorial but are based on scientific facts, and some features of a review paper, without attempting to be comprehensive. These papers have been commissioned by the Editor-in-Chief and reviewed for factual, scientific content by referees.

*Corresponding author. Tel: +81 568 51 6583; fax: +81 568 51 1642.
E-mail address: kokubo@isc.chubu.ac.jp (T. Kokubo).

0142-9612/$ - see front matter © 2006 Elsevier Ltd. All rights reserved.
doi:10.1016/j.biomaterials.2006.01.017

2. History of SBF

In 1980, Hench et al. showed that a SiO_2-rich layer and calcium phosphate film form on the surface of Bioglass when implanted in the body environment, which allows bonding to living bone, and that the in vivo formation of the calcium phosphate film can be reproduced in a buffer solution consisting of Tris hydroxymethylaminomethane and hydrochloric acid (Tris buffer solution) at pH 7.4 [7].

On the other hand, Kitsugi et al. showed that the SiO_2-rich layer does not form on glass-ceramic A–W, but a calcium phosphate layer forms on its surface in the living body, allowing bonding to living bone [8]. Subsequently, Kokubo et al., using micro X-ray diffraction, identified this calcium phosphate layer as crystalline apatite [9]. In addition, in 1990, they showed that the in vivo apatite formation on the surface of glass-ceramic A–W can be reproduced in an acellular SBF with ion concentrations nearly equal to those of the human blood plasma, but not in a Tris buffer solution [10,11]. Kokubo et al. [10] and Hench et al. [12] also independently confirmed the formation of apatite on the surface of Bioglass 45S5-type glass in SBF.

Detailed analysis of the surface apatite formed in SBF, by means of thin film X-ray diffraction (TF-XRD), Fourier transform infrared spectroscopy, scanning electron microscopy and transmission electron microscopy, showed that it was similar to bone mineral in its composition and structure [10,11,13]. As a result, it was speculated that osteoblasts might preferentially proliferate and differentiate to produce apatite and collagen on its surface. Thus formed apatite might bond to the surface apatite as well as to the surrounding bone. Consequently, a tight chemical bond is formed between the material and the living bone through the apatite layer. In contrast, glass-ceramic A–W (Al), which also contains apatite and wollastonite, but in a glassy matrix containing Al_2O_3, and hence does not bond to living bone, did not have apatite form on its surface, both in vivo and in SBF [11,14]. Based on these results, in 1991 it was proposed that the essential requirement for a material to bond to living bone is the formation of bonelike apatite on its surface in the living body and that this in vivo apatite formation can be reproduced in SBF. This means that the in vivo bone bioactivity of a material can be predicted by examining apatite formation on its surface in SBF [6].

It should be noted here that the original SBF used by Kokubo et al. [10] and Hench et al. [12] lacks the SO_4^{2+} ions contained in human blood plasma [15], as shown in Table 1. This was corrected in papers [6,16] published by Kokubo et al. in 1991. Since then, the corrected SBF has been used as "SBF" by many researchers.

It should be also noted here that SBF is a solution highly supersaturated with respect to apatite [17]. It is not easy to prepare clear SBF with no precipitation. Therefore, a detailed recipe for preparation of SBF was reported in 1995 by Cho et al. [18].

However, it can be seen from Table 1 that corrected SBF is still richer in Cl^- ion and poorer in HCO_3^- ion than human blood plasma. In 2003, Oyane et al. tried to correct this difference [19] by preparing a revised SBF (r-SBF) in which the concentrations of Cl^- and HCO_3^- ions were, decreased and increased respectively, to the levels of human blood plasma. However, calcium carbonate has a strong tendency to precipitate from this SBF, as it is supersaturated with respect to not only apatite, but also calcite [20]. In 2004, Takadama et al. proposed a newly improved SBF (n-SBF) in which they decreased only the Cl^- ion concentration to the level of human blood plasma, leaving the HCO_3^- ion concentration equal to that of the corrected SBF (c-SBF) [21]. This improved SBF was compared with the corrected, i.e., conventional, c-SBF in its stability and the reproducibility of apatite formation on synthetic materials. Both SBFs were subjected to round robin testing in ten research institutes. As a result, it was confirmed that the c-SBF does not differ from n-SBF in stability and reproducibility [21]. Through this round robin testing, the method for preparing c-SBF was carefully checked and refined so that the SBF could be easily prepared. This refined recipe for preparing SBF is given in Appendix A of this paper, accompanied with procedure of apatite-forming ability test.

In 2003, conventional SBF with the refined recipe was proposed to the Technical Committee ISO/TC150 of International Organization for Standardization as a solution for in vitro measurement of apatite-forming ability of implant materials and is being discussed by the committee.

Table 1
Ion concentrations of SBFs and human blood plasma

	Ion concentration (mM)							
	Na^+	K^+	Mg^{2+}	Ca^{2+}	Cl^-	HCO_3^-	HPO_4^{2-}	SO_4^{2-}
Human blood plasma [15]	142.0	5.0	1.5	2.5	103.0	27.0	1.0	0.5
Original SBF	142.0	5.0	1.5	2.5	148.8	4.2	1.0	0
Corrected SBF (c-SBF)	142.0	5.0	1.5	2.5	147.8	4.2	1.0	0.5
Revised SBF (r-SBF)	142.0	5.0	1.5	2.5	103.0	27.0	1.0	0.5
Newly improved SBF (n-SBF)	142.0	5.0	1.5	2.5	103.0	4.2	1.0	0.5

3. Qualitative correlation of apatite formation in SBF with in vivo bone bioactivity

As described above, a glass in the Na_2O–CaO–SiO_2–P_2O_5 system named Bioglass 45S5 has apatite form on its surface in SBF [10]. This glass was confirmed to bond to living bone through a calcium phosphate layer [7]. Glasses in the Na_2O–CaO–B_2O_3–Al_2O_3–SiO_2–P_2O_5 system were also found to have a calcium phosphate layer form on their surfaces in SBF [22]. These glasses were also confirmed to bond to living bone though a calcium phosphate layer in vivo [22].

Ceravital®-type glass-ceramic containing apatite was also found to form apatite on its surface in SBF [16] and was confirmed to bond to living bone through a calcium phosphate layer in vivo [16]. Glass-ceramic A–W forms apatite on its surface in SBF, as shown in Fig. 1 [11] and Fig. 2 [13], and was confirmed to bond to living bone through the apatite layer in vivo, as shown in Fig. 3 [9,23]. In contrast, as described above, glass-ceramic A–W (Al) does not form an apatite layer on its surface in SBF [11], does not have apatite form on its surface in vivo and does not bond to living bone [14]. The apatite forming ability of Bioverite®-type glass-ceramic containing apatite and phlogopite has not been examined in SBF, but it has been confirmed to bond to living bone through a calcium phosphate layer [24].

Sintered hydroxyapatite was also found to have apatite form on its surface in SBF [25,26] and was confirmed to bond to living bone through an apatite layer in vivo [23]. Apatite/β-tricalcium phosphate biphasic ceramic was also found to have an apatite layer form on its surface in SBF [4] and was confirmed to bond to living bone through the apatite layer in vivo [4]. Calcium sulfate was also found to form an apatite on its surface in SBF as well as in vivo [27].

For composites, a composite in which glass-ceramic A–W particles are dispersed in a polyethylene matrix was also found to have apatite form on its surface in SBF [28] and bonded to living bone [29]. For all these materials, apatite formation on their surfaces in SBF is well correlated with their in vivo bone bioactivities.

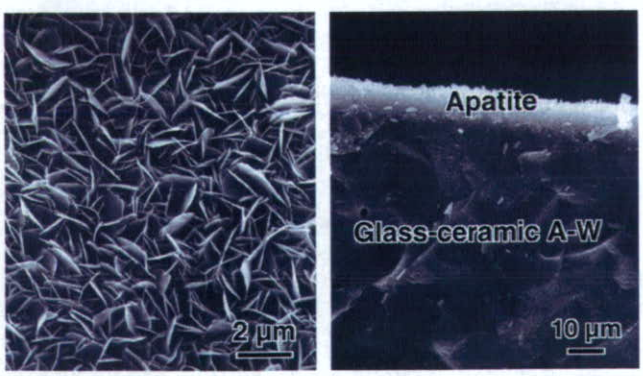

Fig. 1. Scanning electron micrograph of surface (left) and cross section (right) of apatite layer formed on glass-ceramic A–W in SBF [11].

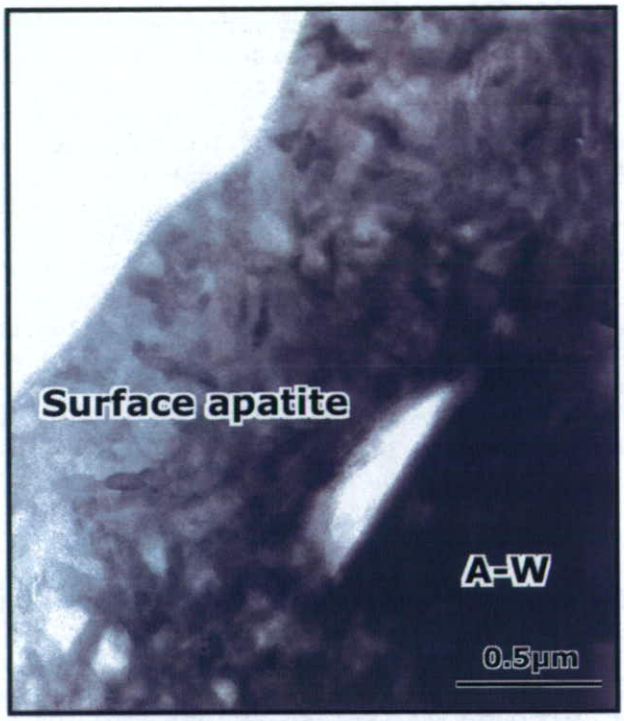

Fig. 2. Transmission electron micrograph of cross section of apatite layer formed on glass-ceramic A–W in SBF [13].

Fig. 3. Transmission electron micrograph of interface between glass-ceramic A–W and rat tibia [23].

However, both β-tricalcium phosphate and natural calcite do not have apatite form on their surfaces in SBF [30,31] or in vivo. [32–34], but despite this, they bond to living bone [32–34]. These results might be related to the high resorbability of these materials. In contrast, natural abalone shell has apatite form on its surface in SBF [31], but does not bond to living bone [35], which might be attributed to antibody reactions to proteins in the shell.

In some reports, SBF with ion concentrations 1.5 times those of SBF (1.5 SBF) has been used when evaluating the in vivo bone bioactivity of a material. There is, however, no correlation between apatite formation on a material in 1.5 SBF with its in vivo bone bioactivity.

It can be said from these results that a material able to have apatite form on its surface in SBF can bond to living bone through the apatite layer formed on its surface in the living body, as long as the material does not contain any substance that induces toxic or antibody reactions.

4. Quantitative correlation of apatite formation in SBF with in vivo bone bioactivity

In 1995, Kim et al. [36] showed that P_2O_5-free Na_2O–CaO–SiO_2 glasses of a wide compositional range have apatite form on their surfaces in SBF, and their apatite forming abilities vary largely with their compositions: i.e. the soaking time in SBF required for apatite formation on their surfaces increased form 0.5 d to longer than 28 d with SiO_2 contents increasing from 50.0 to 70.0 mol% with equal molar concentrations of Na_2O and CaO. Granular particles of these glasses were implanted into holes in rabbit tibiae. The depth of bone growth from the periphery to the interior of the holes at 3 and 6 weeks after implantation increased with the increasing apatite-forming ability of the glasses in SBF at the respective implantation times, as shown in Fig. 4 [37]. The apatite-forming abilities of hydroxyapatite (HA), glass-ceramic A–W and Bioglass in SBF is reported to increase with the order HA < A–W < Bioglass [10,25]. According to Oonishi et al., the depth of bone growth from the periphery to the interior of holes filled with these materials in the tibiae of rabbit also increased in the order HA < A–W < Bioglass [38].

It can be said from these results that the degree of ability for apatite to form on the surface of a material in SBF can predict the degree of in vivo bone bioactivity of the material. A material able to form apatite on its surface in SBF in a short period bonds to living bone in a short period, as a result of apatite formation on its surface in a shorter period within the living body.

5. Development of novel bioactive materials based on apatite formation in SBF

It was shown that CaO and P_2O_5-based glasses in the system CaO–SiO_2–P_2O_5 do not have apatite form on their surfaces in SBF, whereas it forms on CaO and SiO_2-based

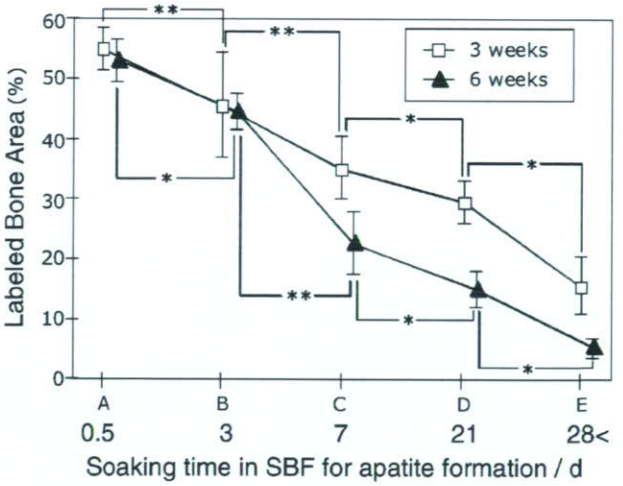

Fig. 4. Dependence of bone formation in a hole of rat tibia filled with glasses on apatite-forming ability of glasses in SBF. Apatite-forming ability increases with decreasing soaking time in SBF for apatite formation [37]. $^*p<0.05$, $^{**}p<0.001$.

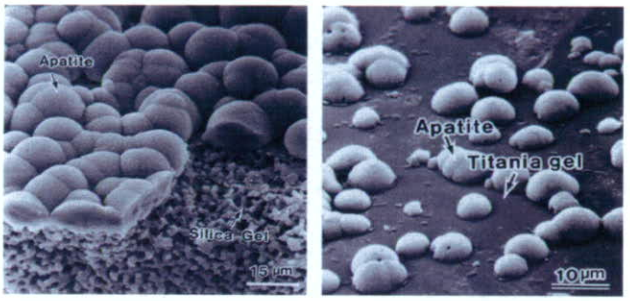

Fig. 5. Scanning electron micrograph of apatite formed on silica gel (left) and titania gel (right) in SBF [46,47].

glasses [39]. The apatite forming ability of a CaO–SiO_2 glass in SBF decreased with the addition of Fe_2O_3 to the glass, and increased with the addition of Na_2O or P_2O_5 [40]. These results then correlated well with in vivo bone bioactivity of the glasses [41,42]. Based on these results, a bioactive ferrimagnetic glass-ceramic containing magnetite in a CaO–SiO_2-based glassy matrix was developed [43,44]. This glass-ceramic can be used as thermoseeds for hyperthermic treatment of cancer [45].

Among the metallic oxide gels prepared using a sol–gel method, those consisting of SiO_2 [46], TiO_2 [47], ZrO_2 [48], Nb_2O_5 [49] and Ta_2O_5 [50] were found to have apatite form on their surfaces in SBF, as shown in Fig. 5, but apatite did not form on gels consisting of Al_2O_3 [47]. These results indicated that Si–OH, Ti–OH, Zr–OH, Nb–OH and Ta–OH groups on the surfaces of these gels are effective for inducing apatite formation on their surfaces in the body environment.

Based on these results, it was speculated that if titanium metal, its alloys and tantalum metal form a sodium titanate or tantalate layer on their surfaces by treatment with a NaOH solution and subsequent heat treatment, they could

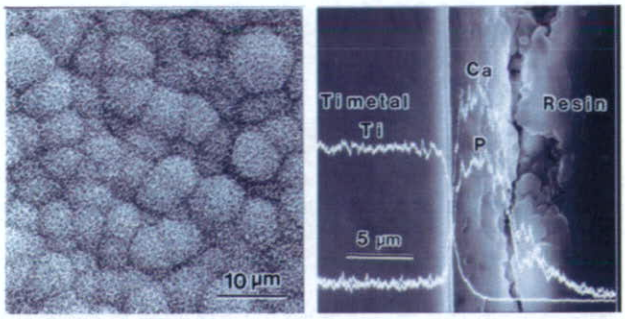

Fig. 6. Scanning electron micrograph of surface (left) and cross section (right) of apatite layer layer formed on NaOH- and heat-treated Ti metal in SBF [51].

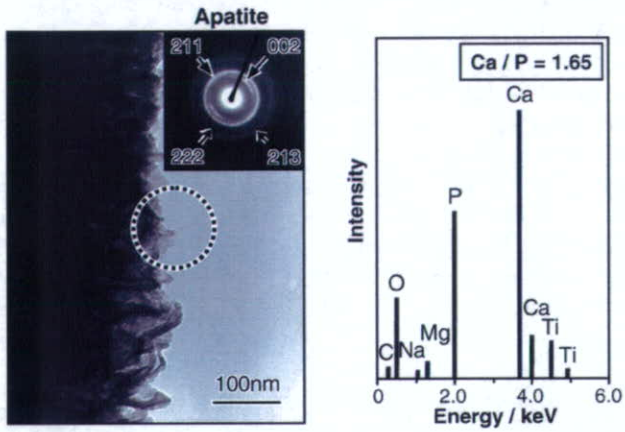

Fig. 7. Transmission electron micrograph (left) and energy dispersive X-ray spectrum (EDX) (right) of apatite formed on NaOH- and heat-treated Ti metals in SBF (dotted circle: area of electron diffraction and EDX analysis) [33].

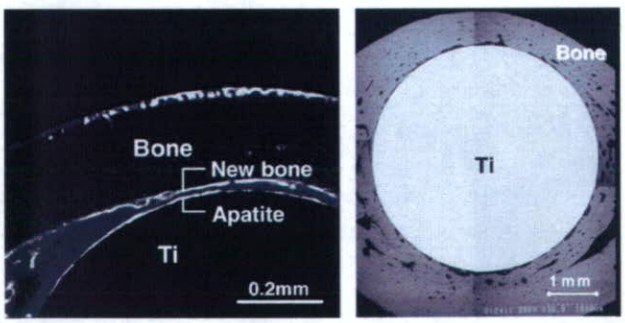

Fig. 8. Confocal laser scanning micrograph (left) and scanning electron micrograph (right) of cross section of NaOH- heat-treated Ti metal rod implanted into rabbit femur for 3 (left) and 12 (right) weeks [54].

form an apatite on their surfaces in SBF, and tightly bond to living bone through the apatite layer formed on their surfaces in the living body. Thus, treated metals had apatite form on their surfaces in SBF [51–53], as shown in Figs. 6 and 7, as well as in vivo [54,55] and, as expected, were tightly bonded to living bone, as shown in Fig. 8 [54]. The bioactive titanium metal thus developed has been applied to artificial hip joints, and a clinical trail of 70 patients has successfully concluded.

6. Conclusion

It is apparent from the results described above that a material able to have apatite form on its surface in SBF has apatite produced on its surface in the living body, and bonds to living bone through this apatite layer. This relationship holds as long as the material does not contain a component that induces toxic or antibody reactions. There are a few materials that directly bond to living bone without the formation of detectable apatite on their surfaces. Despite this limitation, examination of apatite formation on the surface of a material in SBF is useful for predicting the in vivo bone bioactivity of the material, not only qualitatively but also quantitatively. This method can be used for screening bone bioactive materials before animal testing and the number of animals used and the duration of animal experiments can be remarkably reduced by using this method, which can assist in the efficient development of new types of bioactive materials.

Appendix A. Recipe for preparing simulated body fluid (SBF) and procedure of apatite-forming ability test

A.1. Preparation of simulated body fluid (SBF)

A.1.1. Reagents for SBF

The following powder reagent grade chemicals have to be stocked in a desiccator. Ion-exchanged and distilled water is used for the preparation of SBF:

(1) sodium chloride (NaCl),
(2) sodium hydrogen carbonate ($NaHCO_3$),
(3) potassium chloride (KCl),
(4) di-potassium hydrogen phosphate trihydrate ($K_2HPO_4.3H_2O$),
(5) magnesium chloride hexahydrate ($MgCl_2.6H_2O$),
(6) calcium chloride ($CaCl_2$),
(7) sodium sulfate (Na_2SO_4),
(8) Tris-hydroxymethyl aminomethane: ($(HOCH_2)_3CNH_2$) (Tris),
(9) 1M (mol/l) Hydrochloric Acid, 1M-HCl,
(10) pH standard solution, (pH 4, 7 and 9).

A.1.2. Ion concentrations of SBF

The ion concentrations of SBF are shown in Table A1.

A.1.3. Preparation procedure of SBF

Since SBF is supersaturated with respect to apatite, an inappropriate preparation method can lead to the precipitation of apatite in the solution. Always make sure that the preparing solution is kept colorless and transparent and that there is no deposit on the surface of the bottle. If any precipitation occurs, stop preparing SBF, abandon the

solution, restart from washing the apparatus and prepare SBF again.

In order to prepare 1000 ml of SBF, first of all, put 700 ml of ion-exchanged and distilled water with a stirring bar into 1000 ml plastic beaker. Set it in the water bath on the magnetic stirrer and cover it with a watch glass or plastic wrap. Heat the water in the beaker to 36.5 ± 1.5 °C under stirring.

Dissolve only the reagents of 1st to 8th order into the solution at 36.5 ± 1.5 °C one by one in the order given in Table A2, taking care of the indications in the following list. The reagents of 9th (Tris) and 10th order (small amount of HCl) are dissolved in the following process of pH adjustment:

(a) In preparation of SBF, glass containers should be avoided, but a plastic container with smooth surface and without any scratches is recommended, because apatite nucleation can be induced at the surface of a glass container or the edge of scratches. If the container has scratches, replace it by a new one.
(b) Never dissolve several reagents simultaneously. Dissolve a reagent only after the preceding one (if any) is completely dissolved.
(c) Since the reagent $CaCl_2$, which has great effect on precipitation of apatite, takes usually granular form and takes much time to dissolve on granule at a time, completely dissolve one before initiation of dissolution of the next.
(d) Measure the volume of 1M-HCl by cylinder after washing with 1M-HCl.
(e) Measure the hygroscopic reagents such as KCl, $K_2HPO_4 \cdot 3H_2O$, $MgCl_2 \cdot 6H_2O$, $CaCl_2$, Na_2SO_4 in as short a period as possible.

Set the temperature of the solution at 36.5 ± 1.5 °C. If the amount of the solution is smaller than 900 ml, add ion-exchanged and distilled water up to 900 ml in total.

Insert the electrode of the pH meter into the solution. Just before dissolving the Tris, the pH of the solution should be 2.0 ± 1.0.

With the solution temperature between 35 and 38 °C, preferably to 36.5 ± 0.5 °C, dissolve the reagent Tris into the solution little by little taking careful note of the pH change. After adding a small amount of Tris, stop adding it and wait until the reagent already introduced is dissolved completely and the pH has become constant; then add more Tris to raise the pH gradually. When the pH becomes 7.30 ± 0.05, make sure that the temperature of the solution is maintained at 36.5 ± 0.5 °C. With the solution at 36.5 ± 0.5 °C, add more Tris to raise the pH to under 7.45.

Note 1: Do not add a large amount of Tris into the solution at a time, because the radical increase in local pH of the solution can lead to the precipitation of calcium phosphate. If the solution temperature is not within 36.5 ± 0.5 °C, add Tris to raise the pH to 7.30 ± 0.05, stop adding it and wait for the solution temperature to reach 36.5 ± 0.5 °C.

Note 2: The pH shall not increase over 7.45 at 36.5 ± 0.5 °C, taking account of the pH decrease with increasing solution temperature (the pH falls about 0.05/°C at 36.5 ± 1.5 °C).

When the pH has risen to 7.45 ± 0.01, stop dissolving Tris, then drop 1M-HCl by syringe to lower the pH to

Table A1
Nominal ion concentrations of SBF in comparison with those in human blood plasma

Ion	Ion concentrations (mM)	
	Blood plasma	SBF
Na^+	142.0	142.0
K^+	5.0	5.0
Mg^{2+}	1.5	1.5
Ca^{2+}	2.5	2.5
Cl^-	103.0	147.8
HCO_3^-	27.0	4.2
HPO_4^{2-}	1.0	1.0
SO_4^{2-}	0.5	0.5
pH	7.2–7.4	7.40

Table A2
Order, amounts, weighing containers, purities and formula weights of reagents for preparing 1000 ml of SBF

Order	Reagent	Amount	Container	Purity (%)	Formula weight
1	NaCl	8.035 g	Weighing paper	99.5	58.4430
2	$NaHCO_3$	0.355 g	Weighing paper	99.5	84.0068
3	KCl	0.225 g	Weighing bottle	99.5	74.5515
4	$K_2HPO_4 \cdot 3H_2O$	0.231 g	Weighing bottle	99.0	228.2220
5	$MgCl_2 \cdot 6H_2O$	0.311 g	Weighing bottle	98.0	203.3034
6	1.0M-HCl	39 ml	Graduated cylinder	—	—
7	$CaCl_2$	0.292 g	Weighing bottle	95.0	110.9848
8	Na_2SO_4	0.072 g	Weighing bottle	99.0	142.0428
9	Tris	6.118 g	Weighing paper	99.0	121.1356
10	1.0M-HCl	0–5 ml	Syringe	—	—

7.42±0.01, taking care that the pH does not decrease below 7.40. After the pH has fallen to 7.42±0.01, dissolve the remaining Tris little by little until the pH has risen to ⩽7.45. If any Tris remains, add the 1M-HCl and Tris alternately into the solution. Repeat this process until the whole amount of Tris is dissolved keeping the pH within the range of 7.42–7.45. After dissolving the whole amount of Tris, adjust the temperature of the solution to 36.5±0.2 °C. Adjust the pH of the solution by dropping 1M-HCl little by little at a pH of 7.42±0.01 at 36.5±0.2 °C and then finally adjust it to 7.40 exactly at 36.5 °C on condition that the rate of solution temperature increase or decrease is less than 0.1 °C/min.

Remove the electrode of the pH meter form the solution, rinse it with ion-exchanged and distilled water and add the washings into the solution.

Pour the pH-adjusted solution from the beaker into 1000 ml volumetric flask. Rinse the surface of the beaker with ion-exchanged and distilled water and add the washings into the flask several times, fixing the stirring bar with a magnet as if to prevent it from falling into the volumetric flask.

Add the ion-exchanged and distilled water up to the marked line (it is not necessary to adjust exactly, because the volume becomes smaller after cooling), put a lid on the flask and close it with plastic film.

After mixing the solution in the flask, keep it in the water to cool it down to 20 °C.

After the solution temperature has fallen to 20 °C, add the distilled water up to the marked line.

A.1.4. Confirmation of ion concentrations of SBF

Prepared SBF should have the ion concentrations shown in Table A1. In order to confirm the ion concentrations of the SBF, chemical analysis of the SBF is recommended, because SBF is a metastable solution supersaturated with respect to apatite.

Note: It is also recommended that the apatite-forming ability of standard glasses should be examined in the prepared SBF. Chemical compositions of the standard glasses are shown in Table A3. When standard glasses A–C are soaked in SBF, an apatite layer should be detected by thin-film X-ray diffraction and/or scanning electron microscopy after soaking for 12, 24 and 120 h, respectively.

Table A3
The compositions of the standard glasses in the SiO_2–Na_2O–CaO system

Standard glass	Composition (mol%)		
	SiO_2	Na_2O	CaO
A	50	25	25
B	55	22.5	22.5
C	60	20	20

A.1.5. Preservation of SBF

Prepared SBF should be preserved in a plastic bottle with a lid put on tightly and kept at 5–10 °C in a refrigerator. The SBF shall be used within 30 d after preparation.

A.2. Procedure of apatite-forming ability test

A.2.1. Soaking in SBF

For dense materials, measure the specimen dimensions and calculate the surface area with an accuracy of 2 mm^2 for a thin plate.

Calculate the volume of SBF that is used for testing using the following Eq. (1):

$$V_s = S_a/10, \quad (1)$$

where V_s is the volume of SBF (ml) and S_a is the apparent surface area of specimen (mm^2).

For porous materials, the volume of SBF should be greater than the calculated V_s.

Put the calculated volume of SBF into a plastic bottle or beaker. After heating the SBF to 36.5 °C a specimen should be placed in the SBF as shown in Fig. A1. The entire specimen should be submerged in the SBF.

Note: In rare cases, apatite may homogeneously precipitate in the SBF and can be deposited on the surface of a specimen. Therefore, it is recommended that the specimens be placed in the SBF as shown in Fig. A1(a) or Fig. A1(b). In case of placement as shown in Fig. A1 (b), apatite formation should be examined for the lower surface of the specimen.

After soaking at 36.5 °C for different periods within 4 weeks in the SBF, take out the specimen from the SBF and gently wash it with pure water. The specimen should be dried in a desiccator without heating.

Note 1: Bone bonding materials usually form apatite on their surfaces within 4 weeks.

Note 2: A specimen, once taken out of SBF and dried, should not be soaked again.

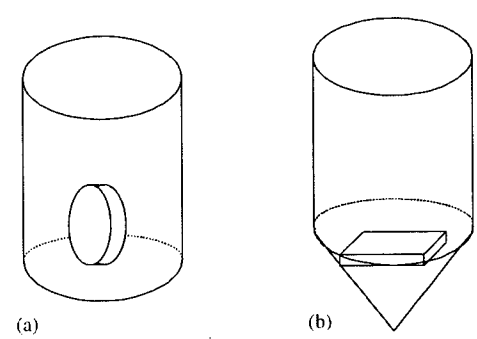

Fig. A1. A specimen in the SBF (Examples).

A.2.2. Surface characterization

Examine the surface of a specimen by TF-XRD and/or scanning electron microscope (SEM) until apatite is detected.

Note 1: The TF-XRD measurement is to be performed in the range of 3–50° in 2 theta (θ) using CuK_α ($\lambda = 0.15405$ nm) radiation as the source at a rate of 2°/min and with 1° glancing angle against the incident beam on the specimen surface.

Note 2: The dried specimen for SEM observation should be thinly metal-coated to induce electro conductivity. The SEM photos should be taken both at high magnifications (around 10,000) and low magnifications (around 1000).

Note 3: The TF-XRD measurement can clearly identify the apatite formation on the specimen. The SEM observation can observe the material formation on the specimen, but can not identify whether the formed material is apatite or not. Therefore, the SEM observation should be accompanied with TF-XRD measurement. However, formed apatite grains and layers have characteristic features to be identified, and the apatite formation is sometimes estimated only on SEM.

References

[1] Hench LL, Splinter RJ, Allen WC, Greenlee TK. Bonding mechanisms at the interface of ceramics prosthetic materials. J Biomed Mater Res 1972;2:117–41.

[2] Jarcho M, Kay JI, Gummaer RH, Drobeck HP. Tissue, cellular and subcellular events at a bone–ceramic hydroxyapatite interface. J Bioeng 1977:179–92.

[3] Rejda BJ, Peelen JGJ, de Groot K. Tricalcium phosphate as a bone substitute. J Bioeng 1977;1:93–7.

[4] Legeros RZ, Lin S, Rohanizadeh R, Mijares D, Legeros JP. Biphasic calcium phosphate bioceramics: preparation, properties and applications. J Mater Sci Mater Med 2003;14:201–9.

[5] Kokubo T, Shigematsu M, Nagashima Y, Tashiro M, Nakamura T, Yamamuro T, et al. Apatite- and wollastonite-containing glass-ceramic for prosthetic application. Bull Inst Chem Res Kyoto Univ 1982;60:260–8.

[6] Kokubo T. Bioactive glass ceramics: properties and applications. Biomaterials 1991;12:155–63.

[7] Ogino M, Ohuchi F, Hench LL. Compositional dependence of the formation of calcium phosphate films on bioglass. J Biomed Mater Res 1980;14:55–64.

[8] Kitsugi T, Nakamura T, Yamamuro T, Kokubo T, Shibuya T, Takagi M. SEM-EPMA observation of three types of apatite-containing glass ceramics implanted in bone: the variance of a Ca, P-rich layer. J Biomed Mater Res 1987;21:1255–71.

[9] Kokubo T, Ohtsuki C, Kotani S, Kitsugi T, Yamamuro T. Surface structure of bioactive glass-ceramic A–W implanted into sheep and human vertebra. In: Heimke G, editor. Bioceramics, vol. 2. Cologne: German Ceramic Society; 1990. p. 113–21.

[10] Kokubo T, Kushitani H, Sakka S, Kitsugi T, Yamamuro T. Solutions able to reproduce in vivo surface-structure change in bioactive glass-ceramic A–W. J Biomed Mater Res 1990;24:721–34.

[11] Kokubo T, Ito S, Huang T, Hayashi T, Sakka S, Kitsugi T, et al. Ca, P-rich layer formed on high-strength bioactive glass-ceramic A–W. J Biomed Mater Res 1990;24:331–43.

[12] Filgueiras MR, Torre GL, Hench LL. Solution effects on the surface reactions of a bioactive glass. J Biomed Mater Res 1993;27:445–53.

[13] Ohtsuki C, Aoki Y, Kokubo T, Bando Y, Neo M, Nakamura T. Transmission electron microscopic observation of glass-ceramic A–W and apatite layer formed on its surface in a simulated body fluid. J Ceram Soc Japan 1995;103:449–54.

[14] Kitsugi T, Yamamuro T, Nakamura T, Kokubo T. The bonding of glass ceramics to bone. Int Orthop 1989;13:199–206.

[15] Gamble JE. Chemical anatomy, physiology and pathology of extracellular fluid. Cambridge, MA: Harvard University Press; 1967. p. 1–17.

[16] Ohtsuki C, Kushitani H, Kokubo T, Kotani S, Yamamuro T. Apatite formation on the surface of Ceravital-type glass-ceramic in the body. J Biomed Mater Res 1991;25:1363–70.

[17] Neuman W, Neuman M. The chemical dynamics of bone mineral. IL: University of Chicago; 1958. p. 34.

[18] Cho S, Nakanishi K, Kokubo T, Soga N, Ohtsuki C, Nakamura T, et al. Dependence of apatite formation on silica gel on its structure: effect of heat treatment. J Am Ceram Soc 1995;78:1769–974.

[19] Oyane A, Kim HM, Furuya T, Kokubo T, Miyazaki T, Nakamura T. Preparation and assessment of revised simulated body fluids. J Biomed Mater Res 2003;65A:188–95.

[20] Oyane A, Onuma K, Ito A, Kim HM, Kokubo T, Nakamura T. Formation and growth of clusters in conventional and new kinds of simulated body fluids. J Biomed Mater Res 2003;64A:339–48.

[21] Takadama H, Hashimoto M, Mizuno M, Kokubo T. Round-robin test of SBF for in vitro measurement of apatite-forming ability of synthetic materials. Phos Res Bull 2004;17:119–25.

[22] Anderson ÖH, Karlsson KH. On the bioactivity of silicate glass. J Non-Cryst Solids 1991;129:145–51.

[23] Neo M, Kotani S, Nakamura T, Yamamuro T, Ohtsuki C, Kokubo T, et al. A comparative study of ultrastructures of the interfaces between four kinds of surface-active ceramic and bone. J Biomed Mater Res 1992;26:1419–32.

[24] Höland W, Vogel W, Naumann K. Interface reaction between machinable bioactive glass-ceramics and bone. J Biomed Mater Res 1985;19:303–12.

[25] Kokubo T, Kushiyani M, Ebisawa Y, Kitsugi T, Kotani S, Oura K, et al. Apatite formation on bioactive ceramics in body environment. In: Oonishi, Aoki H, Sawai K, editors. Bioceramics. Tokyo: Ishiyaku EuroAmerica; 1988 p. 157–62.

[26] Kim HM, Himeno T, Kawashita M, Kokubo T, Nakamura T. The mechanism of biomineralization of bone-like apatite on synthetic hydroxyapatite: an in vitro assessment. J R Soc Interface 2004;1:17–22.

[27] Chan H, Mijares D, Ricci JL. In vitro dissolution of calcium sulfate: evidence of bioactivity. Transactions of the seventh world biomaterials congress,. 2004. p. 627.

[28] Judasz JA, Best SM, Bonfield W, Kawashita M, Miyata N, Kokubo T, et al. Apatite-forming ability of glass-ceramic apatite-wollastonite-polyethylene composites: effect of filler content. J Mater Sci: Mater Med 2003;14:489–95.

[29] Judasz JA, Ishii S, Best SM, Kawashita M, Neo M, Kokubo T, et al. Bone-bonding ability of glass-ceramic apatite-wollastonite-polyethylene composites. Transactions of the seventh world biomaterials congress, 2004. p. 665.

[30] Ohtsuki C, Kokubo T, Neo M, Kotani S, Yamamuro T, Nakamura T, et al. Bone-bonding mechanism of sintered β-$3CaO$-P_2O_5. Phos Res Bull 1991;1:191–6.

[31] Ohtsuki C, Aoki Y, Kokubo T, Fujita Y, Kotani S, Yamamuro T. Bioactivity of limestone and abalone shell. Transactions of the 11th annual meeting of Japanese Society for Biomaterials, 1989. p. 12.

[32] Kotani S, Fujita Y, Kitsugi T, Nakamura T, Yamamuro T. Bone bonding mechanism of β-tricalcium phosphate. J Biomed Mater Res 1991;25:1303–15.

[33] Neo M, Nakamura T, Ohtsuki C, Kokubo T, Yamamuro T. Apatite formation of three kinds of bioactive materials at early stage in vivo: a comparative study by transmission electron microscopy. J Biomed Mater Res 1993;27:999–1006.